Light Propagation in a Weakly Perturbed Expanding Universe

by

Uroš Seljak

B.S., University of Ljubljana (1989)
S.M. University of Ljubljana (1991)

Submitted to the Department of Physics
in partial fulfillment of the requirements for the degree of

Doctor of Philosophy

at the

MASSACHUSETTS INSTITUTE OF TECHNOLOGY

May 1995

© Uroš Seljak, MCMXCV. All rights reserved.

Author . . . .
Department of Physics
May 18, 1995

Certified by. . . . .
Edmund Bertschinger
Associate Professor
Thesis Supervisor

Accepted by . . . .
George F. Koster
Chairman, Departmental Committee on Graduate Students

MASSACHUSETTS INSTITUTE
OF TECHNOLOGY

JUN 2 6 1995

Science

Light Propagation in a Weakly Perturbed Expanding Universe

by

Uroš Seljak

Abstract

I investigate the theoretical aspects of light propagation through the universe in the framework of a weakly perturbed Robertson-Walker model. Assuming that the metric perturbations are small, which is a valid approximation almost everywhere in our universe, I derive the general equations of light propagation using the geodesic equations in a perturbed space-time. These equations are used to study the temperature and spatial distribution of light, with the goal of comparing the theoretical predictions to the actual observations.

The first part of the thesis is dedicated to the study of temperature distribution in the cosmic microwave background (CMB). I start with primary contributions using the linear theory analysis, which is an excellent approximation if the anisotropies were generated when the universe recombined at a redshift around 1100. I present a treatment of perturbations based on a tight-coupling approximation, which simplifies the equations significantly and enables one to identify the physical processes and parameters, while at the same time preserving an accuracy of 10-20% when compared to the exact results. Using this model I identify 6 physical parameters that can be determined from the measurements of CMB anisotropies. Next I analyze the effect of nonlinear clustering or Rees-Sciama effect on CMB anisotropies, which might make a significant secondary contribution and complicate the simple picture given by the linear theory. I find that for a wide class of CDM models the effect is of order $\Delta T/T \sim 10^{-7} - 10^{-6}$ and is at least an order of magnitude below the contribution from the primary anisotropies.

In the second part of the thesis I investigate how the spatial distribution of light is affected by the matter distribution in the universe through the gravitational lensing effect. I investigate the weak lensing effect on the positions and time delays between multiple images of strong gravitational lenses. I show that although the absolute deviation of an image position relative to its unperturbed position can be of the order of arcminutes, relative positions and time delays are only weakly perturbed, of the order of a few percent. Finally I investigate the weak lensing effect on the correlations in the CMB anisotropies. The effect is most likely negligible on degree angular scales,

but becomes more important on arcminute scales and leads to the smoothing of sharp features in the CMB angular power spectrum.

Thesis Supervisor: Edmund Bertschinger
Title: Associate Professor
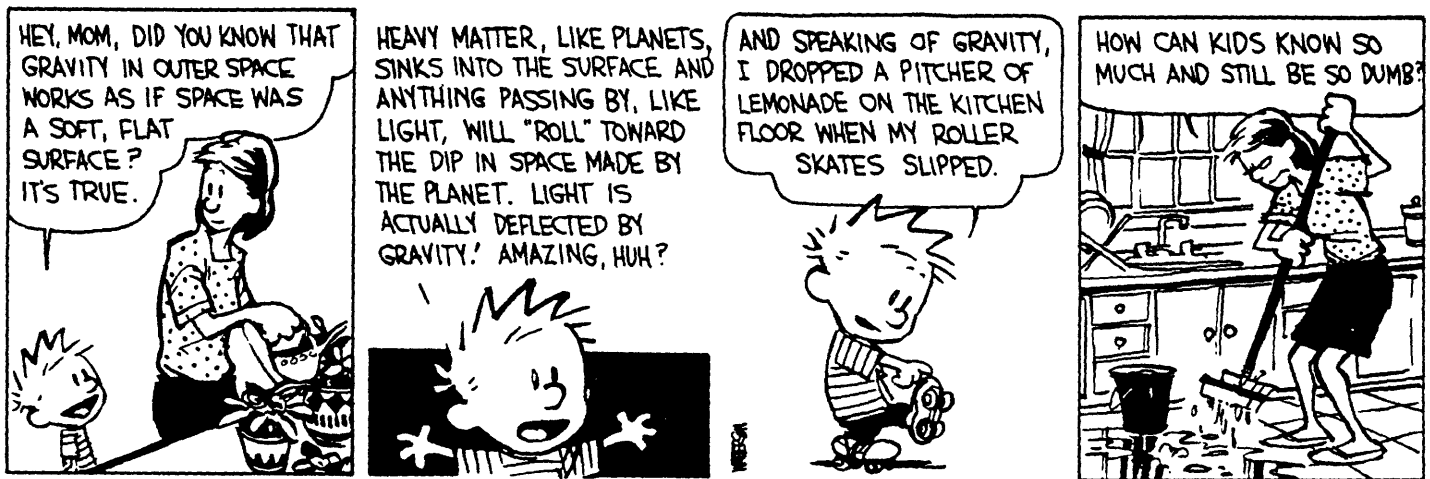
(Borrowed from *The indispensable Calvin and Hobbes* by Bill Waterson.)

Acknowledgments

Finally it is time to write the famous last words. As it usually happens, there is too little time and too many people to mention you all. Let me try to do my best and I apologize to all of you who were inadvertently left out.

First I would like to thank my advisor, Ed Bertschinger. His encouragement and support followed me throughout my stay here at MIT and was crucial for the succesful completion of this thesis. Most of what I learned about astrophysics and cosmology is due to him, either through our numerous conversations or through his several excellent lecture notes. I would especially like to thank him for encouraging me to work independently, which allowed me to fulfill a great goal in my life: to see how is it to be a creative scientist.

There are many others at MIT that I would like to thank: Bhuvnesh, Jim, John, Lam, Mark, Shep and all the other fellow graduate students, post-docs and professors for numerous discussions about life inside and outside the academic world.

I am also grateful to Jackie Hewitt for reading and commenting upon this thesis and to Peggy Berkovitz and Chris Naylor for being so helpful from the beginning to the end.

Two people ouside MIT had a profound impact on this thesis. I would like to thank Dick Bond for his encouragement and both Dick and Nick Kaiser for their scientific papers from which I often sought inspiration for my work.

Most importantly, I would like to thank to my parents, who were with me all the time, despite the great distance between us. Our weekly telephone conversations helped reminding me that I still have a home back there. And finally, I thank Petra, whose love and companionship made these years so memorable.

Contents

List of Figures

Chapter 1

Introduction

In the last two decades there has been a vast increase in the amount of observations of light sources at cosmological distances. Most important among these are quasars with measured redshifts up to $z \approx 5$, faint blue galaxies with redshifts around $z \approx 1$ and cosmic microwave background (CMB), which is thought to be the earliest observable light source in our universe with $z \approx 1100$. As the light emitted by these sources is propagating through the universe, it gets affected by the intermediate mass distribution, so that both the energy and the direction of the photons change. The first effect has its most important manifestation in the temperature fluctuations of CMB, which can provide important information on the state of our universe at a very early stage of its evolution. The second effect has its most spectacular evidence in the observations of gravitational lenses (GL), where light from a single source (usually a bright quasar) is deflected and observed in multiple images. This effect can also provide cosmologically important information not accessible in any other way. The purpose of this thesis is to provide a unifying description of these phenomena, which is general enough to encompass all the relevant processes, yet it is also simple enough to clearly display different physical and geometrical features that can affect the observable properties of light.

The framework within which I derive all the necessary formalism is given by the weakly-perturbed expanding universe. I assume that in an average sense our universe is well described by a Robertson-Walker metric, which is the most general metric

under the assumptions of a homogeneous and isotropic expanding universe. In the presence of matter inhomogeneities the metric becomes perturbed. The metric perturbations are not directly measurable and their amplitudes depend on the choice of the coordinate system (i. e., they are gauge dependent). While at early stages of evolution the amplitudes are small independent of the coordinate system, at late times this is not true anymore, especially in the regime where the rms density fluctuations are much larger than the mean density in the universe. However, there exists a particular coordinate system in which the metric perturbations reduce in an appropriate limit to the dimensionless Newtonian potential. This assures that the metric perturbations are small even in the late stages of evolution, because the Newtonian gravitational potential for bound objects with nonrelativistic velocities v is of the order of $v^2/c^2 \ll 1$. From the assumption that metric perturbations are small (and, for consistency, that bulk velocities are small) one can derive a complete set of relativistic perturbation theory equations, which include Einstein's equations describing the relation between metric perturbations and energy-momentum tensor, geodesic and Boltzmann equations describing the evolution of photons and neutrinos and fluid equations describing the evolution of fluids in the universe. In this picture light propagation is described using linearized general relativity, while the sources of gravitational field are evolved using full equations of motion, which may be nonlinear in the density field. The only place where this procedure breaks down is near a black hole, where gravitational potential becomes large and a perturbative approach in the gravitational potential is no longer valid. In this case one may explicitly solve for the photon trajectory using the Kerr metric around the black hole, connecting it to the weakly perturbed metric far enough from it. Since only a negligible fraction of lines of sight pass near a black hole one may ignore this case entirely, if one is interested in average statistical properties of light distribution.

The first part of this thesis is dedicated to the study of CMB anisotropies. The measurement of anisotropy by COBE-DMR (Smoot et al. 1992) and subsequent measurements both by COBE and smaller scale measurements indicate that the early universe, while very smooth, did have small-amplitude fluctuations ($\sim$ 1 part in

10^5) in the metric. Large angular scale experiments such as COBE probe the initial conditions of our universe, in particular the amplitude and the slope of the primordial power spectrum (Smoot et al. 1992; Górski et al. 1994). These scales could also provide information on the geometry and the matter content of the universe (Kofman & Starobinski 1985; Kamionkowski & Spergel 1994; Sugiyama & Silk 1995). The geometry manifests itself through a different set of eigenfunctions on a curved space, whereas the matter content introduces a time dependent potential in the transition period from $\Omega \approx 1$ to $\Omega \ll 1$. However, theoretical interpretation of measurements on these scales is complicated by so-called cosmic variance, expressing the fact that we can only observe one particular realization of the sky temperature distribution, and this intrinsically limits the accuracy with which these parameters can be estimated using the large angular scale measurements alone.

Small angular scale measurements suffer less from the cosmic variance, although their interpretation is complicated by the microphysics during recombination and possible reionization of the universe. Once a fluctuation scale enters the acoustic horizon prior or during recombination, it is acted on by processes that arise due to the coupling of baryons to photons. Theoretical models often give wildly different predictions for the anisotropy power spectra when the parameter values are only slightly changed, while some combinations of parameters seem to provide nearly identical spectra (e.g. Bond et al. 1994). The calculations based on a coupled system of Einstein, fluid and Boltzmann equations (presented in Appendix A) are rather time consuming and the physical processes that lead to the fluctuations are difficult to separate. In Chapter 2 I present a simplified treatment of isentropic (adiabatic) perturbations, based on a tight-coupling approximation between photons and baryons, which is a good approximation before the universe recombined. This model gives a 10-20% accuracy when compared to the exact results and so is accurate enough that it can be used for a quantitative analysis of various models, yet it is also simple enough that it can clearly separate between most different physical processes that affect the CMB fluctuations (a similar analytic approach has recently been developed by Hu & Sugiyama 1995). Using this model I identify 6 physical parameters that can be

determined with CMB anisotropies, provided that extensive mapping of microwave sky on a few arcminute scale is obtained. These parameters are the primorial slope of the power spectrum, baryon and matter densities, Hubble constant, Thomson optical depth from recombination until today and Silk damping scale (I assume here that the seventh parameter, the overall amplitude of fluctuations, has already been accurately measured by COBE; additional parameters are introduced if tensor fluctuations make a significant contribution to CMB, as predicted by some theories of inflation, or if the primordial power spectrum is not a pure power law).

The simple picture presented in chapter 2 is valid as long as the main contribution to the CMB fluctuations arises from the primary fluctuations during the recombination epoch ($z \approx 1100$), when the fluctuations were linear and can in principle be calculated with arbitrary precision. This picture could be complicated by the presence of nonlinear contributions to the anisotropies, arising from the late stages of evolution. Not only are these determined by different physical processes, in most cases they are also less well known and are difficult to calculate even in well specified models. In chapter 3 I present the analysis of a particular nonlinear contribution known as the Rees-Sciama effect, which is caused by a potential changing in time during the nonlinear stages of evolution and was first pointed out by Rees & Sciama (1968). If a given structure was static and at rest in comoving coordinates then the gravitational blueshift for a photon falling into the structure potential would be exactly cancelled by the redshift of the photon climbing out of the potential. If the structure is collapsing or moving the two contributions do not cancel out and the photon suffers a net energy change, which translates into a temperature fluctuation in a given direction. This effect is independent of the frequency, because it is caused by the gravitational shifting of photons. This means that it cannot be separated from the primary contribution using a multi-frequency spectral information and the only way to separate it from the primary signal is to specify its spatial distribution. It is therefore important to analyze the angular power spectrum of the Rees-Sciama effect to determine if it is significant compared to the primary signal on any angular scale. If this indeed turns out to be the case, then one would need to calculate

higher order statistics and/or produce real space simulated maps to effectively separate the two contributions. In Chapter 3 I concentrate on the first task with the purpose of identifying which are the angular scales where the Rees-Sciama effect can be important.

The imprint of nonlinear clustering on the CMB has been analyzed by several authors after the seminal work by Rees & Sciama (1968). Most of this previous work gave only partial answers, studying for example isolated structures, such as clusters, superclusters and voids (Rees & Sciama 1968; Kaiser 1982; Nottale 1984; Thompson & Vishniac 1987; Panek 1992; Martínez-González & Sanz 1990; Chodorowski 1992, 1994; Arnau, Fullana & Sáez 1994), quasi-linear (Martínez-González, Sanz & Silk 1992) or strongly nonlinear regimes (Martínez-González, Sanz & Silk 1994). Recently, Tuluie & Laguna (1995) presented a detailed N-body analysis of a standard CDM model using ray-tracing of photons. This approach has the advantage of producing real maps of $\Delta T/T$, thereby allowing one to identify the non-gaussian features that contribute to the Rees-Sciama effect. Unfortunately such approach is also computationally expensive and the results have a rather small dynamic range, in the case of Tuluie & Laguna (1995) being limited by the number of traced photons and by the resolution of their 64^3 PM simulation. For this reason these authors only present results on degree angular scales for one particular model.

The approach I present in Chapter 3 similarly uses output of N-body simulation to calculate the effect and so properly includes both linear and nonlinear stages of evolution, however instead of using ray-tracing the power spectrum of Rees-Sciama contribution is calculated from particle positions and velocities, without having the need to actually trace photons through a dedicated N-body simulation. This allows one to use already existing N-body simulations with a large dynamic range. By matching the N-body results with the second order perturbation theory calculation the results can be extended to the scales larger than the size of the simulation box. This way the accessible angular range extends from the largest angles down to arcminute scales and covers most of the observationally interesting scales. Another advantage of the approach used here is that one can analyze several different CDM

14

models with the same N-body simulation by rescaling its time and/or length, which allows one to assess the sensitivity of the Rees-Sciama effect to the change in the shape and/or amplitude of the power spectrum.

The second part of the thesis is dedicated to the study of gravitational lenses and their importance in determining the cosmological parameters. The possibility of studying the physical parameters of the distant universe using gravitational lenses (GL) was first suggested in the 1960s. In particular, Refsdal (1964, 1966) pointed out that one could determine the masses of galaxies and the Hubble constant using the observed image properties, most notably their positions, magnifications and time delays between images of the same source. The latter became especially interesting after the time delay in the system 0957+561 was measured (e.g. Vanderriest et al. 1989; Lehár et al. 1992) and a value of H_0 derived (Rhee 1991; Roberts et al. 1991). Alcock & Anderson (1985, 1986), Watanabe, Sasaki & Tomita (1992) and Sasaki (1993) criticized the method, arguing that large scale structure might significantly affect the time delay. Unfortunately, their arguments were only qualitative and could not give realistic predictions of the amplitude of fluctuations. In light of this many workers in the field have taken an optimistic view and assumed that the derived value of H_0 gives at least an upper limit to the actual value (e.g. Borgeest & Refsdal 1984). These arguments are based on the fact that mass density is always positive and therefore always focuses the rays. However, this is only correct in Newtonian gravity and becomes invalid in cosmological applications, where underdensities such as voids give an effective negative mass density (e.g. Nityananda & Ostriker 1984). In general, the question whether large scale structure could significantly affect the measured properties of the lens has remained largely unanswered.

In Chapter 4 I investigate how the large-scale structure changes the direction of light through the weak lensing effect and how this affects the positions and time delays between the multiple images of strong gravitational lenses. The calculation is done using linearized general relativity and is described in detail in Appendix B. For simplicity I restrict the discussion to the case of a linear theory in a flat space, although the equations presented in Appendix B and Chapter 5 can be used to analyze the

15

more general case. A similar approach has previously been used by Linder (1990a,b), Kaiser (1992), Cayón et al. (1993a,b) and Pyne & Birkinshaw (1995). An alternative method, based on optical scalars, has been developed by Gunn (1967) and applied to the ellipticity and magnification correlation function calculations by Babul & Lee (1991), Blandford et al. (1991) and Miralda-Escudé (1991).

In Chapter 5 I study the weak lensing effect on the CMB fluctuations, thereby connecting the two subjects analyzed in previous chapters. This effect has been investigated in the past by several groups (Blanchard & Schneider 1987; Cole & Efstathiou 1989; Sasaki 1989; Tomita & Watanabe 1989; Cayón, Martínez-González & Sanz 1993a,b; Bassett et al. 1994; Fukushige et al. 1994). Using different approaches these authors came to very different conclusions about the importance of the effect. Cole & Efstathiou (1989) used a nonlinear CDM model and found a small effect on the CMB. Cayón et al. (1993a,b) used a linear model and found an appreciable effect on arcminute angular scales for some models. On degree angular scales they also found a negligible effect. On the other hand, using different approaches such as the Dyer-Roeder distance-redshift relation or simplified N-body simulations Bassett et al. (1994) and Fukushige et al. (1994) found a significant effect even on degree angular scales.

There are two main shortcomings of these studies that do not allow one to draw a firm conclusion on the importance of the effect. First, the studies are based on a particular cosmological model and the results could change significantly if the model is changed. While some groups (e.g. Cole & Efstathiou 1989; Cayón, Martínez-González & Sanz 1993a,b) attempted to assess this uncertainty by presenting results for different viable cosmological models, others (e.g. Bassett et al. 1994; Fukushige et al. 1994) used models that do not allow a direct comparison with existing observational constraints and thus may not even be realistic models. A second shortcoming of previous studies is that they do not fully include the evolution of large-scale structure in their models. While Cole & Efstathiou (1989) calculated the effect only at late epochs when the matter is in the nonlinear regime, Cayón et al. (1993a,b) only included the linear evolution, whereas Bassett et al. (1994) and Fukushige et al. 1994

neglected any evolution at all and assumed that the universe did not change from a certain redshift until today.

In Chapter 5 I attempt to provide a more realistic answer on the importance of the lensing effect on the CMB by using observational constraints on large-scale structure distribution and properly including its evolution. The method used is similar to the one used in Chapter 4 and presented in more detail in Appendix B. This work differs from previous studies in that I also include the nonlinear effects by modelling the power spectrum evolution in the nonlinear regime and I extend the calculation to the case of an open (or closed) universe. This allows to calculate the lensing effect in any specified cosmological model. The estimate of the effect on the CMB is based on observational constraints on the power spectrum and on the ellipticity correlations of distant galaxies, which enables one to assess its magnitude in a relatively model independent way. The results are presented in terms of the CMB anisotropy power spectrum, in contrast to earlier work, which emphasized the effect on the correlation function. This allows to present the effect independent of the observational strategy and provides a clear display of the limitation imposed by lensing on extracting the true anisotropy power spectrum.

Bibliography

[1] Alcock, C., & Anderson, N. 1985, ApJ, 291, L29

[2] Alcock, C., & Anderson, N. 1986, ApJ, 302, 43

[3] Arnau, J. V., Fullana, M. J., & Sáez, D. 1994, MNRAS, 268, L17

[4] Babul, A., & Lee, M. H. 1991, MNRAS, 250, 407

[5] Bassett, B. A. C. C., Dunsby, P. K. S. & Ellis, G. F. R. 1995, Phys. Rev. D, to be published

[6] Blanchard, A. and Schneider, J., 1987, A&A, 184, 1

[7] Blandford, R. D., Saust, A. B., Brainerd, T. G., & Villumsen, J. V. 1991, MNRAS, 251, 600

[8] Bond, J. R., Crittenden, R., Davis, R. L., Efstathiou, G., & Steinhard, P. J. 1994, Phys. Rev. Lett., 72, 13

[9] Borgeest, U., & Refsdal, S. 1984, A&A, 141, 318

[10] Cayón, L., Martínez-González, E., & Sanz, J. L. 1993a, ApJ, 403, 471

[11] Cayón, L., Martínez-González, E., & Sanz, J. L. 1993b, ApJ, 413, 10

[12] Chodorowski, M. J. 1992, MNRAS, 259, 218

[13] Chodorowski, M. J. 1994, MNRAS, 266, 897

[14] Cole, S. and Efstathiou, G., 1989, MNRAS, 239, 195

[15] Fukushige, T., Makino, J., & Ebisuzaki, T. 1994, ApJ436, L107

[16] Górski, K. M. et al. 1994, ApJ, 430, L89

[17] Gunn, J. E. 1967, ApJ, 147, 61

[18] Hu, W., & Sugiyama, N. 1995, Phys. Rev. D, 51, 2599

[19] Kaiser, N. 1982, MNRAS, 198, 1033

[20] Kamionkowski, M. & Spergel, D. N. 1994, ApJ, 432, 7

[21] Kofman, L., & Starobinsky, A. 1985, Sov. Astron. Lett., 11, 271

[22] Lehár, J., Hewitt, J. N., Roberts, D. H., & Burke, B. F. 1992, ApJ, 384, 453

[23] Linder, V. E. 1990a, MNRAS, 243, 353

[24] Linder, V. E. 1990b, MNRAS, 243, 362

[25] Martínez-González, E., Sanz, J. L., & Silk, J. 1990, ApJ, 355, L5

[26] Martínez-González, E., Sanz, J. L., & Silk, J. 1992, Phys. Rev. D, 46, 4196

[27] Martínez-González, E., Sanz, J. L., & Silk, J. 1994, ApJ, 436, 1

[28] Miralda-Escudé, J. 1991, ApJ, 380, 1

[29] Nityananda, R., & Ostriker, J. P. 1984, J. Ap. Astr., 5, 235

[30] Nottale, L. 1984, MNRAS, 206, 713

[31] Panek, M. 1992, ApJ, 388, 225

[32] Rees, M. J., & Sciama, D. W. 1968, Nature, 517, 611

[33] Refsdal, S. 1964, MNRAS, 128, 307

[34] Refsdal, S. 1966, MNRAS, 132, 101

[35] Rhee, G. 1991, Nature, 350, 211

[36] Roberts, D., H., Lèhar, J., Hewitt, J. N., & Burke, B., F. 1991, Nature, 352, 43

[37] Sasaki, M. 1989, MNRAS, 240, 415

[38] Sasaki, M. 1993, Prog. Theor. Phys. 90, 753

[39] Smoot, G. F. et al. 1993, ApJ, 396, L1

[40] Sugiyama, N. & Silk, J. 1994, Phys. Rev. Lett., 731, 509

[41] Thompson, K. L., Vishniac, E. T. 1987, ApJ, 313, 517

[42] Tuluie, R., & Laguna, P. 1995, submitted to ApJ

[43] Vanderriest, C., Schneider, J., Herpe, G., Chevreton, M., Moles, M., & Wlerick, G. 1989, A&A, 215, 1

[44] Tomita, K. and Watanabe, K., 1989, Prog. Theor. Phys., 82, 563

[45] Watanabe, K., Sasaki, M., & Tomita, K. 1992, ApJ, 394, 38

Chapter 2

A Two-fluid Approximation for Calculating the Cosmic Microwave Background Anisotropies

In this Chapter[1] I present a tight-coupling approximation for calculating the temperature fluctuations in CMBR. The approximation is applied to the case where the initial fluctuations are isentropic (i.e. constant in entropy, also incorrectly called adiabatic), which are the initial conditions usually predicted by physical theories (e.g. by inflation). I use this approximation to predict CMB power spectra in various cosmological models and to identify the key physical processes and parameters that can affect the CMB measurements.

2.1   Method

The method for computing the CMB anisotropies is based on the line-of-sight integration along the photon past light cone (Appendix A). I assume that the photons and baryons are tightly coupled prior to recombination, which allows a simple two-fluid description of perturbations (Peebles & Yu 1970). The analysis is restricted to

---

[1]Based on the publication ApJ, 435, L87 (1994).

the linear perturbation theory of adiabatic perturbations and I neglect any possible vector and tensor contributions. Different theoretical models are compared using the angular power spectrum of CMB anisotropies C_l, as defined in Appendix A.

The temperature fluctuation $\Delta_\gamma(\vec{n})$ in the direction $\vec{n}$ can be expressed as a line-of-sight integral as in equation (A.24),

$$\Delta_\gamma(\vec{n}) = \int_0^{\tau_0} [\dot{\mu}(\phi + \frac{\delta_\gamma}{4} + \vec{n} \cdot \vec{v_b}) + 2\dot{\phi}]e^{-\mu}d\tau. \tag{2.1}$$

In the limit of infinitely thin last-scattering surface (valid for wavelengths much larger than the width of the last scattering surface) the function $\dot{\mu}e^{-\mu}$ approaches to the Dirac delta-function $\delta(\tau - \tau_{rec})$, where τ_{rec} denotes the conformal time at recombination. I neglected neutrino and photon anisotropic stresses, which from equation (A.11) implies $\psi = \phi$. This is a reasonable approximation on scales smaller than the Hubble scale η^{-1}, but leads to $\sim 10\%$ effect on C_l on large scales, where neutrino anisotropic stress cannot be neglected. Equation (A.24) then reduces to

$$\Delta_\gamma(\vec{n}) = \phi(\tau_{rec}) + \frac{\delta_\gamma(\tau_{rec})}{4} + \vec{n} \cdot \vec{v_b}(\tau_{rec}) + 2 \int_{\tau_{rec}}^{\tau_0} \dot{\phi}(\tau)d\tau. \tag{2.2}$$

In this limit the angular moments given by equation (A.29) reduce to the following expression,

$$\begin{aligned} C_l &= (4\pi)^2 \int_0^\infty k^2 P(k) T(k) D_l^2 dk \\ D_l &= (\phi + \frac{\delta_\gamma}{4}) j_l(k\tau_{rec}) + v_b j_l'(k\tau_{rec}) + 2 \int_{\tau_{rec}}^{\tau_0} d\tau j_l(k\tau)\dot{F}(\tau), \end{aligned} \tag{2.3}$$

where $P(k)$ is the primordial power spectrum of potential ϕ. Most of the cosmological theories predict that it can be modelled as a power law over a large range of wavelengths, $P(k) \propto k^{n-4}$, where n is the primordial power spectrum index[2]. All the perturbed quantities are evaluated in k-space at τ_{rec}. Anticipating later needs, I I

---

[2]Of course one can always introduce a "designer" initial spectrum that will fit all the observations. This approach is physically unmotivated and leaves little predictive power to our disposal and is not the approach taken here.

introduced the function $T(k)$, which incorporates the damping effects. As discussed in the Appendix A the results presented here will be valid for non-flat universes, provided that the relation between angles and physical sizes is expressed using angular size distances. The last term in equation (2.3) gives the integrated Sachs-Wolfe (ISW) contribution (Sachs & Wolfe 1966). The time dependence of the potential is denoted with $\dot{F}(\tau)$, where $F(\tau)$ is the growth factor for potential, excplicitly given for the case of a vacuum energy dominated universe (Kofman & Starobinsky 1985) and curvature dominated universe (Kamionkowski & Spergel 1994) in Chapter 3. It vanishes in a flat, matter dominated $\Omega_{m0} = 1$ universe, but is present when the universe is in transition epoch from being radiation to being matter dominated (Kodama & Sasaki 1986; see below).

To calculate the anisotropy power spectrum one needs to evaluate the source contributions in equation (2.3) at the epoch of recombination. The photon, baryon and CDM evolution equations in k-space are given in Appendix A. The energy and momentum constraint equations are given by Einstein's equations (A.11) and lead to the equations for ϕ and $\dot{\phi}$,

$$\phi = -\frac{4\pi G a^2}{k^2}(\bar{\rho}\delta + \frac{3\dot{a}\bar{\rho}v}{ak}), \quad \dot{\phi} = -\frac{\dot{a}}{a}\phi + \frac{4\pi G a^2 \bar{\rho}v}{k}, \tag{2.4}$$

where $\bar{\rho}\delta = (\bar{\rho}_\gamma + \bar{\rho}_\nu)\delta_\gamma + \bar{\rho}_b\delta_b + \bar{\rho}_c\delta_c$ and $\bar{\rho}v = \frac{4}{3}(\bar{\rho}_\gamma + \bar{\rho}_\nu)v_\gamma + \bar{\rho}_b v_b + \bar{\rho}_c v_c$. Here $\bar{\rho}_\gamma$, $\bar{\rho}_\nu$, $\bar{\rho}_b$ and $\bar{\rho}_c$ are the photon, neutrino, baryon and CDM mean densities, respectively. I replaced the neutrino density and velocity perturbations with the corresponding photon perturbations. This becomes invalid on small scales due to the free-streaming of neutrinos, but does not affect significantly the final results. I also neglected the anisotropic stress, polarization and the curvature terms.

The above equations are supplemented by the Friedman's equation (A.6), which at early times (when a possible cosmological constant or curvature term can be neglected) is given by

$$\left(\frac{\dot{a}}{a}\right)^2 = \frac{8\pi G a^2}{3}(\bar{\rho}_\gamma + \bar{\rho}_\nu + \bar{\rho}_b + \bar{\rho}_c). \tag{2.5}$$

The solution to this equation is

$$y \equiv \frac{a}{a_{eq}} = (\alpha x)^2 + 2\alpha x, \qquad x = \left(\frac{\Omega_{m0}}{a_{rec}}\right)^{1/2} \frac{H_0 \tau}{2} \equiv \frac{\tau}{\tau_r}, \qquad (2.6)$$

where $a_{eq} = (\bar{\rho}_{\gamma 0} + \bar{\rho}_{\nu 0})/(\bar{\rho}_{b0} + \bar{\rho}_{c0}) \approx 4.2 \times 10^{-5} \Omega_{m0}^{-1} h^{-2}$ (assuming three flavors of massless neutrinos), $a_{rec}^{-1} \approx 1100$ for the standard recombination, $\alpha^2 \equiv a_{rec}/a_{eq}$, $\Omega_{m0} = \Omega_{b0} + \Omega_{c0}$ is the value of matter density today in units of critical density and h is the value of Hubble constant today in units of 100km/s/Mpc.

I will now assume the tight coupling limit $\mu \gg k$, which is a good approximation on scales larger than the Silk damping scale (Silk 1968, Peebles & Yu 1970). In this case the photons and baryons are coupled into a single fluid with $\delta_b = \frac{3}{4}\delta_\gamma$ and $v_b = v_\gamma$. The fluid equations rewritten in terms of dimensionless time x and dimensionless wavevector $\kappa = k\tau_r$ become

$$\dot{\delta}_c = -\kappa v_c + 3\dot{\phi}, \qquad \dot{v}_c = -\eta v_c + \kappa\phi,$$

$$\dot{\delta}_\gamma = -\frac{4}{3}\kappa v_\gamma + 4\dot{\phi}, \qquad \dot{v}_\gamma = \left(\frac{4}{3} + y_b\right)^{-1}\left[-\eta y_b v_\gamma + \frac{\kappa\delta_\gamma}{3} + \kappa\phi\left(\frac{4}{3} + y_b\right)\right],$$

$$\phi = -\frac{3}{2}(\eta/\kappa)^2(\delta + 3\eta v/\kappa), \qquad \dot{\phi} = -\eta\phi + \frac{3\eta^2 v}{2\kappa},$$

$$\delta = \frac{\delta_\gamma[1 + \frac{3}{4}(y - y_c)] + y_c\delta_c}{1 + y}, \qquad v = \frac{v_\gamma(\frac{4}{3} + y - y_c) + y_c v_c}{1 + y}, \qquad (2.7)$$

where the derivatives are taken with respect to x, $y_b \equiv \frac{\bar{\rho}_b}{\bar{\rho}_\gamma} = [1 + \frac{3 \times 7}{8}(\frac{4}{11})^{4/3}]\frac{\Omega_{b0}}{\Omega_{m0}}y = 1.68\frac{\Omega_{b0}}{\Omega_{m0}}y$, $y_c = \frac{\Omega_{c0}}{\Omega_{m0}}y = (1 - \frac{\Omega_{b0}}{\Omega_{m0}}/1.68)y$ and $\eta = 2\alpha(\alpha x + 1)/(\alpha^2 x^2 + 2\alpha x)$.

Equations (2.7) are a coupled system of 4 first order differential equations.[3] The appropriate initial conditions at $x \ll 1$ (when the universe is radiation dominated) and $\kappa\eta \ll 1$ (when the mode is larger than the Hubble sphere radius) are

$$\phi = 1, \quad \delta_\gamma = -2\phi\left(1 + \frac{3y}{16}\right), \quad \delta_c = \frac{3}{4}\delta_\gamma$$

---

[3]In actual numerical implementation of these equations I find that for a stable numerical integration it is better to compute ϕ using its time evolution in equation (2.7), rather than computing it from the sources.

$$v_\gamma = v_c = -\frac{\kappa}{\eta}\left[\frac{\delta_\gamma}{4} + \frac{2\kappa^2(1+y)\phi}{9\eta^2(\frac{4}{3}+y)}\right].$$ (2.8)

The equations of motion need to be evolved until $x_{rec} = [(\alpha^2 + 1)^{1/2} - 1]/\alpha$. The temperature anisotropy expressed with the dimensionless variables is then given by

$$C_l = 4\pi A \int_0^\infty \kappa^n T(\kappa) d\ln\kappa \left[\left(\left(\phi + \frac{\delta_\gamma}{4} + 2\Delta\phi\right)\right) j_l(\kappa x_0) + v_\gamma j_l'(\kappa x_0)\right]^2,$$ (2.9)

where x_0 is the angular distance to the last-scattering surface in units of τ_r and I assumed $P(k) = Ak^{-3}\kappa^{n-1}$. The term $\Delta\phi = [2 - 8/y(x_{rec}) + 16x_{rec}/y^3(x_{rec})]/10y(x_{rec})$ arises from the ISW effect due to the potential varying with time during the transition period from the radiation dominated to the matter dominated universe (Kodama & Sasaki 1986). Although the potential changes only by 10% during this transition, it nevertheless leads to a significant effect on C_l's in adiabatic models with late matter-radiation transition, because it needs to be compared to the usual Sachs-Wolfe contribution $\phi/3$. For simplicity I dropped the ISW contribution from possible curvature or cosmological constant, which is only important at the lowest values of l.

The damping transfer function $T(\kappa)$ is approximately unity for low values of l ($l < 200$), but gradually decreases afterwards. Its main contributions come from the Silk damping and from the finite width of the last-scattering surface. The first effect can be calculated analytically by expanding equations (A.15) and (A.24) to second order in μ and neglecting the effects of gravity and expansion. In the matter-dominated era one obtains $T(\kappa) \propto \exp(-2\kappa^2 x_s^2)$ (Fugukita, Sugiyama & Unemura 1990), where x_s is the Silk damping scale in units of τ_r, $x_s = 0.6\Omega_{m0}^{1/4}\Omega_{b0}^{-1/2}a_{rec}^{3/4}h^{-1/2}$. The second effect can be analytically estimated by performing the line-of-sight integral in equation (A.24) in the limit where the sources are slowly changing over the timescale on which the visibility function $\dot\mu e^{-\mu}$ is non-negligible (Jørgensen et al. 1994). The visibility function can be approximated as a gaussian $(2\pi\sigma^2 x_{rec}^2)^{-1/2}\exp[-(x-x_{rec})^2/2(\sigma x_{rec})^2]$, where for standard recombination $\sigma \approx 0.03$.[4] In the limit $\kappa_0 x_0 \gg l$ (where κ_0 is the

---

[4]Both σ and a_{rec} are weakly dependent on cosmological parameters. Moreover, the ISW visibility function differs from the Thomson scattering visibility function, which leads to a different damping

wavevector which gives the dominant contribution to C_l), I obtain the damping factor $\exp(-\kappa^2\sigma^2 x_{rec}^2)$. Therefore, the damping effects can be written as

$$T(\kappa) \approx e^{-\kappa^2(2x_s^2+\sigma^2 x_{rec}^2)}. \tag{2.10}$$

This works reasonably well for the standard ionization history. Note however that if the limit $\kappa_0 x_0 \gg l$ is not satisfied, then the damping due to the finite thickness of last-scattering surface is not exponential, but is proportional to κ^{-1}. This will be the case, for example, in reionized models.

Equations (2.7)–(2.10) are all that is needed to evaluate the temperature fluctuations. Although equations (2.7) cannot be solved analytically in general, they have analytic solutions in the limits of small and large κ. In the first limit where the modes are larger than the Hubble sphere radius the amplitude of perturbations at a given time is a constant (Figure 2-1). This gives the standard Sachs-Wolfe expression for CMB fluctuations, as can be verified by evolving the initial conditions in equations (2.8) into the matter-dominated era and neglecting the velocity term in equation (2.9). In the second limit (large κ) the equations can be solved using the WKB approximation and the solution gives the acoustic oscillations of the photon-baryon plasma (Jørgensen et al. 1994; Padmanabhan 1993; Hu & Sugiyama 1995). In the intermediate regime, which is of main interest for us, the equations need to be solved numerically, but the physics can be well understood by the two limits above. As shown in Figure (2-1), equations (2.7) give an excellent approximation to the exact results (obtained by solving a coupled system of Einstein's, fluid and Boltzmann equations, see Appendix A and references therein) over a large range of wavevector κ.

Although the above system of equations is particularly useful for the standard recombination scenarios, it can also be used to calculate anisotropy power spectrum in reionized models. As one can see from equation (A.24), the primary fluctuations will be suppressed by a factor $\exp[-\mu(x_{rec})]$, where $\mu(x_{rec})$ is Thomson opacity at

of the ISW term. Both effects will be neglected here.

recombination. In addition, there will be secondary fluctuations generated at the new last-scattering surface, which can be calculated using the same method as above, except that one needs to replace v_b with v_c in the regime where the Compton drag is negligible. Since the modes larger than the Hubble sphere radius at the new last-scattering surface do not evolve in the matter-dominated regime this simply regenerates the Sachs-Wolfe expression for low values of l. On smaller scales the thick new last-scattering surface damps the secondary fluctuations and in many scenarios these become negligible (although on arcminute scales the second-order terms may become important; see Vishniac 1987). Provided that one is interested in degree angular scales, then the effect of reionization is to suppress the fluctuation power spectrum relative to the large scales by a factor of $\exp[-2\mu(x_{rec})]$.

2.2 Results

The comparison between the approximation presented here and the exact solutions of the perturbed Boltzmann equation (Seljak & Bertschinger 1994) is given in Figure (2-2) for several isentropic cosmological models. All of the multipole moments are normalized relative to C_{10}, which is approximately fixed by the COBE experiment and where the curvature effects and ISW effects due to $\Omega_{m0} \neq 1$ can be neglected. One can see that the agreement is excellent over a large range of l. The deviations at large l arise because of improper treatment of damping effects, while the deviations at small l can be attributed to the neglection of neutrino anisotropic shear. Another effect that introduces small deviations is the dependence of a_{rec} on cosmological parameters, which slightly offsets the position of the peaks. Nevertheless, the approximation correctly predicts the positions and amplitudes of Doppler peaks (also called acoustic or Sakharov oscillations) with a 10-20 % accuracy over most of the parameter range.

Given the high accuracy of this model I may now investigate how the anisotropy power spectrum depends on the cosmological model. The goal is to identify the parameters that can be determined using the CMB measurements and to give a physical understanding of how they affect the anisotropies. In equations (2.7) the free param-

eters are $\alpha = 21.5\Omega_{m0}^{1/2}h$ and $\frac{\Omega_{b0}}{\Omega_{m0}}$. One can replace them with physically more relevant parameters $\Omega_{m0}h^2 = (\alpha/21.5)^2$ and $\Omega_{b0}h^2 = (\alpha/21.5)^2\frac{\Omega_{b0}}{\Omega_{m0}}$. In addition to these two one has the parameters $\mu(x_{rec})$, n, x_0 and x_s. These six parameters will uniquely[5] determine all the CMB power spectra within the approximation. Of the parameters above, n, $\mu(x_{rec})$ and x_s all suppress the power on small scales relative to large scales (for $n < 1$). The suppression is different in the three cases, being proportional to κ^{n-1} (neglecting the possible tensor contribution), $\exp[-\mu(x_{rec})]$ and $\exp(-2\kappa^2 x_s^2)$, respectively. This, in principle, allows to separate the different suppression effects and to determine the three parameters separately. Note that these parameters do not change the positions of the Doppler peaks, only their amplitude. The effects of these parameters are physically transparent and change the positions of the Doppler peaks by a few percent only over their allowed range. I will therefore restrict in the following to the case of $n = 1$ and $\mu(x_{rec}) = 0$. Moreover, Silk damping is important only for large values of l and it can be neglected if one concentrates on the first few Doppler peaks. One is thus left with x_0, $\Omega_{m0}h^2$ and $\Omega_{b0}h^2$, which uniquely determine positions of the Doppler peaks.

The position of the first Doppler peak is determined by the angular size of the acoustic horizon at decoupling, which is proportional to the Hubble radius for small Ω_{b0}. Expressed in terms of variables used here it is proportional to $(1 + \alpha^{-2})^{1/2}x_0$. Since $\alpha \gg 1$ for typical values of $\Omega_{m0}h^2$, the position of the first Doppler peak mainly depends on x_0. Assuming $x_{rec} \ll x_0$ one has $x_0 = (\Omega_{m0}a_{rec})^{-1/2}$ for the model with negligible cosmological constant and $x_0 \approx \Omega_{m0}^{0.09}a_{rec}^{-1/2}$ for the model with negligible curvature. The latter result shows that the first Doppler peak only weakly depends on $\Omega_{\lambda 0} = 1 - \Omega_{m0}$. This is because the angular size distance at large redshifts scales with Ω_{m0} in approximately the same way as does the Hubble sphere radius at decoupling (Vittorio & Silk 1985; Górski & Stompor 1994). This is, however, not true in general and the position of the first Doppler peak depends on Ω_{m0} and $\Omega_{\lambda 0}$ when both curvature and cosmological constant are important. The value of

---

[5] I am assuming that the universe is either open with no cosmological constant or flat with a cosmological constant, in which case Ω_{m0} is the parameter that specifies the two models.

l at which the maximum of the first Doppler peak lies is given approximately by $6x_0$. Figure (2-3a) compares C_l's of curvature and cosmological constant dominated models with those of the flat $\Omega_{m0} = 1$ model at fixed values of $\Omega_{m0}h^2$ and $\Omega_{b0}h^2$. One can see that the position of the first Doppler peak can accurately determine Ω_{m0} in a curvature dominated universe (Kamionkowski, Spergel & Sugiyama 1994), but cannot precisely determine Ω_{m0} in a cosmological constant dominated universe (Bond et al. 1994; Górski & Stompor 1994). However, even in this model the positions of secondary Doppler peaks are already significantly displaced relative to each other when Ω_{m0} changes from 0.25 to 1. This would thus allow independent determination of Ω_{m0} even in a cosmological constant dominated universe, once $\Omega_{m0}h^2$ and $\Omega_{b0}h^2$ are known (see below).

The dependence of the Doppler peak positions and amplitudes on $\Omega_{b0}h^2$ and $\Omega_{m0}h^2$ is more complicated, since both parameters appear in the evolution equations (2.7) and change the properties of acoustic oscillations. The two parameters enter into the equations differently and have different physical effects: $\Omega_{b0}h^2$ is related to the properties of the photon-baryon plasma and determines its effective sound velocity at recombination, whereas $\Omega_{m0}h^2$ is related to the time evolution of the expansion factor, since it determines the epoch of matter-radiation equality. This means that one cannot expect the anisotropy spectra to remain invariant under a certain combination of the two parameters and both $\Omega_{b0}h^2$ and $\Omega_{m0}h^2$ are required for a complete description of the Doppler peaks. Figures (2-3b) and (2-3c) show how the Doppler peaks change when one of the two parameters is changing while the other is held fixed. If one concentrates on the first Doppler peak then it is not possible to determine the two parameters simultaneously, since both increasing $\Omega_{b0}h^2$ and decreasing $\Omega_{m0}h^2$ lead to a higher first Doppler peak. The physical mechanisms that lead to this are different: while an increase in $\Omega_{b0}h^2$ increases the amplitude of the first wave in v_γ and $\phi + \delta_\gamma/4$ (fig. 2-1), a decrease in $\Omega_{m0}h^2$ also leads to an increased ISW contribution. Once the secondary peaks are observed as well, then different effects of the two parameters become significant and allow one to determine the two parameters simultaneously (Figs. 2-3 b,c,d). Figure (2-3d) shows how changing $\Omega_{m0}h^2$ at a fixed value of $\frac{\Omega_{b0}}{\Omega_{m0}}$

affects the multipole moments. Again, since the epoch of matter-radiation equality is changing with $\Omega_{m0}h^2$, one does not expect the multipole moments to remain unchanged and both the approximation and exact calculations confirm this. Therefore, changing h at a fixed Ω_{b0} and Ω_{m0} changes the anisotropy power spectrum.

2.3 Discussion

The approximation for calculating the anisotropy power spectrum presented here is a generalization of the Sachs-Wolfe approximation, which itself is only valid on scales larger than the acoustic horizon at recombination. By modelling the cosmological perturbations as a two-component fluid plasma one can extend this approach to all scales. The approximation is useful both for developing the physical understanding of processes that affect CMB fluctuations, as well as for a quantitative prediction of multipole moments for various cosmological models. While the analysis in this Chapter has been concentrated on the physically better motivated isentropic initial conditions, one can develop an analogous approximation also for isocurvature modes (Hu & Sugiyama 1995). The main approximations used in this model are a two-fluid approximation, neglect of anisotropic shear and polarization, a simplified treatment of Thomson scattering effects, neglection of curvature effects and neglection of vector and tensor contributions. None of these assumptions is essential for the method and one can generalize the approach presented here to obtain exact results (e.g. Appendix A). This will lead to a computationally more demanding system of equations, but the main physical effects that lead to the creation of Doppler peaks will still be determined by the equations presented here.

By rewriting the equations in their dimensionless form I identified all the dimensionless parameters that affect the anisotropy power spectra in this approximation. Measurements of CMB fluctuations can in the lowest order only determine these parameters. For example, neutrinos enter into the equations indirectly through the Friedmann equation (2.5) and through the energy-momentum constraint equations (2.4). The presence of a massive neutrino only weakly changes these equations and

the resultant multipole moments are almost indistinguishable from the ones with the massless neutrino. Therefore, the question of whether neutrino has a mass has little hope to be answered using the CMB measurements (Ma & Bertschinger 1995).

The most interesting aspect of the CMB power spectra is the peculiar pattern of the Doppler peaks, which allows a simultaneous determination of $\Omega_{b0}h^2$ and $\Omega_{m0}h^2$. This would provide an independent test of nucleosynthesis prediction of $\Omega_{b0}h^2$ (e.g. Walker et al. 1991) and would also constrain the parameter space on Ω_{m0} and h. In addition, the position of the first Doppler peak determines Ω_{m0} in curvature dominated models. In cosmological constant dominated models the position of the first Doppler peak does not allow one to determine Ω_{m0} accurately, but positions of secondary Doppler peaks could be used to constrain Ω_{m0}. Another way to break the degeneracy between Ω_{m0}, Ω_{b0} and h is to determine the Silk damping scale x_s, which depends only on these three parameters and cannot be expressed as a combination of $\Omega_{b0}h^2$ and $\Omega_{m0}h^2$. This would require a separation of Silk damping from the damping due to the finite thickness of the last-scattering surface in reionized models and from the $n < 1$ suppression of small scales relative to large scales (including the possible tensor contribution). This is possible, because the three effects suppress the small scale power differently. Thus, a combination of CMB measurements over a large range of angles could be used to separately determine the baryon mass density, matter mass density and the Hubble constant in a wide class of physically motivated cosmological models.

Bibliography

[1] Bode, P., & Bertschinger, E. 1995, preprint astro-ph 9504040

[2] Bond, J. R., Crittenden, R., Davis, R. L., Efstathiou, G., & Steinhard, P. J. 1994, Phys. Rev. Lett., 72, 13

[3] Fugukita, M., Sugiyama, N., & Unemura, M. 1990, ApJ, 358, 28

[4] Górski, K. M., & Stompor, K. M. 1994, ApJ, 422, L41

[5] Hu, W., & Sugiyama, N. 1995, Phys. rev. D, 51, 2599

[6] Jørgensen, H.E., Kotok, E., Naselsky, P., & Novikov, I. 1994, A&A, 294, 639

[7] Kamionkowski, M. & Spergel, D. N. 1994, ApJ, 432, 7

[8] Kamionkowski, M., Spergel, D. N., & Sugiyama, N. 1994, ApJ, 426, L57

[9] Kodama, H., & Sasaki, M. 1986, Int. J. Mod. Phys. A1, 265

[10] Kofman, L., & Starobinsky, A. 1985, Sov. Astron. Lett., 11, 271

[11] Ma, C. P., & Bertschinger, E. 1995, ApJ, to be published

[12] Padmanabhan, T. 1993, Structure Formation in the Universe, Cambridge: Cambridge University Press

[13] Peebles, P. J. E., & Yu, I. T. 1970, ApJ, 162, 815

[14] Sachs, R. K., & Wolfe, A. M. 1966, ApJ, 147, 73

[15] Seljak, U., & Bertschinger, E. 1994, in "Present and Future of the Cosmic Microwave Background", eds. J. L. Sanz, E. Martinez-Gonzalez, & L. Cayon (1994)

[16] Silk, J. 1968, ApJ, 151, 459

[17] Vishniac, E. T. 1987, ApJ, 322, 597

[18] Vittorio, N., & Silk, J. 1985, ApJ, 297, L1

[19] Walker, T. P., Steigman, G., Schramm, D. N., Olive, K. A., & Kang, H. 1991, ApJ, 376, 51
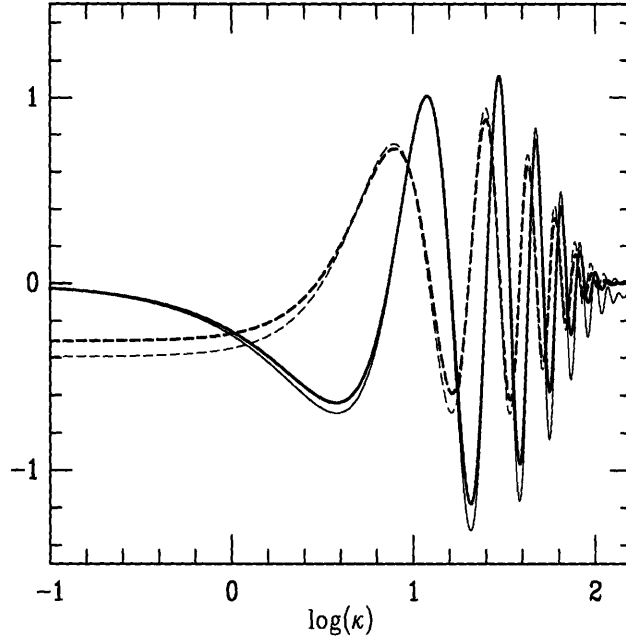
Figure 2-1: Comparison between this approximation (thick lines) and exact solution (thin lines) for v_γ (solid lines) and $\phi + \delta_\gamma/4$ (dashed lines) as a function of κ. Silk damping has been included according to the expression in the text. Parameter values are $\Omega_{b0} = 0.05$, $h = 0.5$ and $\Omega_{m0} = 1$.
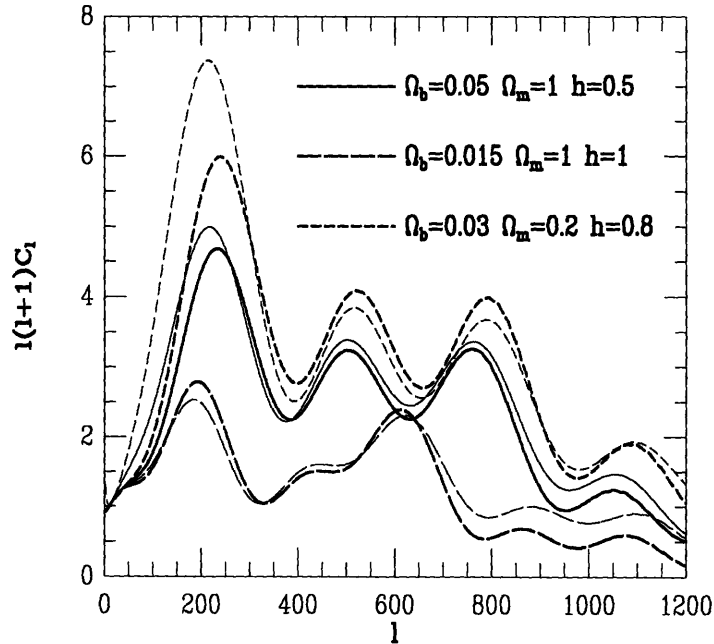
Figure 2-2: Comparison of anisotropy power spectra between this approximation (thick lines) and exact solution (thin lines) as a function of multipole moment l for several different cosmological models. The spectra in this and next figure are normalized relative to C_{10}.

34
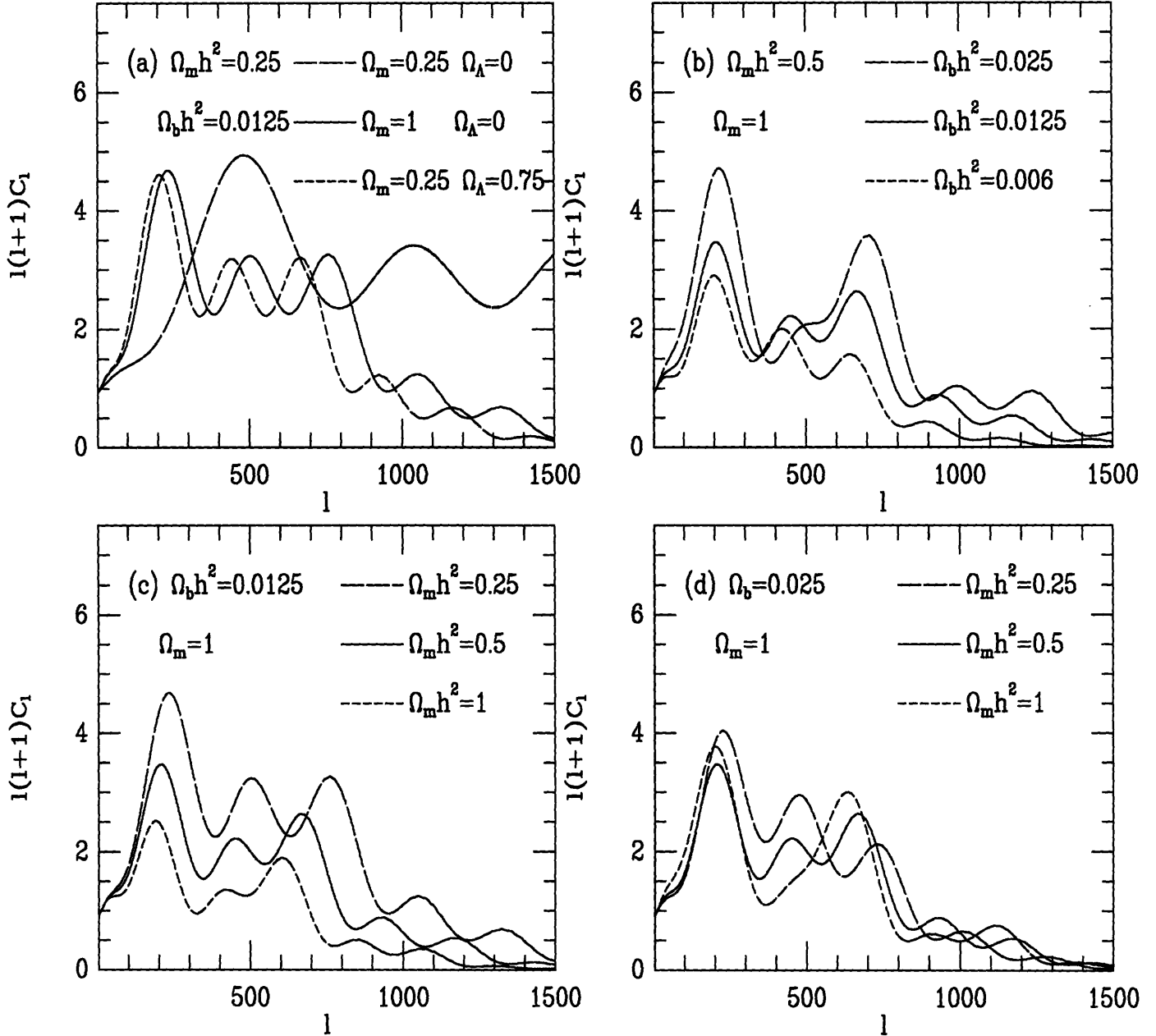
Figure 2-3: Anisotropy power spectra as a function of multipole moment l for different cosmological models. In (a) curvature and cosmological constant dominated models with $\Omega_{m0} = 0.25$ are compared to $\Omega_{m0} = 1$ model. In (b) $\Omega_{m0}h^2$ is fixed at 0.5 and $\Omega_{b0}h^2$ is varying, whereas in (c) $\Omega_{b0}h^2$ is fixed at the nucleosynthesis value and $\Omega_{m0}h^2$ is varying. In (d) Ω_{b0}/Ω_{m0} is fixed and $\Omega_{m0}h^2$ is varying. In (b), (c) and (d) $\Omega_{m0} = 1$. In all cases varying the parameter changes the pattern of Doppler peaks.

Chapter 3

Rees-Sciama Effect in CDM Cosmogonies

If the visibility function $\dot{\mu}\exp(-\mu)$ is sharply peaked around recombination, then the CMB temperature anisotropy can be written as a contribution from the last-scattering surface plus a line-of-sight integral arising from the time dependent potential (integrated Sachs-Wolfe term in equation 2.2). In the previous Chapter I investigated the contributions to the anisotropies from the last-scattering surface. In this Chapter I turn the attention to the integrated Sachs-Wolfe effect arising from the nonlinear clustering of matter in the late epochs of structure formation, also called the Rees-Sciama (1968) effect (hereafter RS).

3.1 Power Spectrum of Potential Time Derivative

As shown in Chapter 2 one can approximate the CMB anisotropy as

$$\Delta_\gamma(\vec{n}) = \Delta_\gamma(\vec{n})_{rec} + \int_{\tau_{rec}}^{\tau_0} 2\dot{\phi}d\tau, \tag{3.1}$$

where τ_{rec} is the recombination time and $\Delta_\gamma(\vec{n})_{rec}$ is the primary contribution to the CMB anisotropy created at the last scattering surface. The second term is the in-

tegrated Sachs-Wolfe contribution and depends on the time derivative (with respect to the conformal time τ) of the gravitational potential along the line-of-sight. In this expression I neglected the Thomson damping term $\exp(-\mu)$, which is valid if the dominant contributions to the integrated Sachs-Wolfe term come from low redshifts where the universe is optically thin. The integrated Sachs-Wolfe term and in particular its nonlinear contribution is usually associated with the RS effect.

The magnitude of the RS effect is studied in terms of the angular power spectrum C_l (defined in Appendix A), which describes the rms amplitude as a function of angular scale. Although for nonlinear processes studied here the power spectrum is not a sufficient statistic, it nevertheless provides a useful tool to compare contributions between various processes on the same angular scale, provided that they are statistically uncorrelated. Here I compare the anisotropies arising from the Rees-Sciama effect with the primary anisotropies arising on the last-scattering surface. The two contributions are spatially well separated and can be treated as uncorrelated. In addition to this there might be other secondary contributions to $\Delta T/T$, such as the Sunyaev-Zeldovich effect or Vishniac effect (see e.g. Appendix A; Persi et al. 1995), both of which are caused by the clustering of large-scale structure just like the Rees-Sciama effect and are thus not necessary uncorrelated with it. I will not discuss this general case here, since the primary goal is to answer the question: can the RS effect dominate over the primary contribution on any angular scale? If this indeed turns out to be the case, then a more detailed study of the RS effect would be needed, including the analysis of its higher order moments (e.g. Munshi, Souradeep & Starobinski 1994; Mollerach et al. 1995), producing real sky maps (e.g. Tuluie & Laguna 1995) and cross-correlating the RS effect with other (Vishniac, SZ) secondary sources that are important on a given scale.

On small angular scales the Rees-Sciama contribution to the CMB anisotropy power spectrum can be written as (equation A.35)

$$C_l^{(RS)} = 32\pi^3 \int_0^{\tau_0} \frac{P_{\dot\phi}(l/r,\tau)d\tau}{r^2}. \tag{3.2}$$

In order to compute the RS effect $P_{\dot\phi}(k,\tau)$ needs to be specified as a function of time and scale. The potential is related to the density through the first of Einstein's equations (A.11), which reduces on small scales in the matter dominated epoch to the Poisson equation. Its Fourier transform is

$$- k^2\phi = \frac{3}{2}\Omega_{m0}H_0^2 a^{-1}\delta. \qquad (3.3)$$

In the linear regime $\dot\phi$ is readily evaluated using the well known solution for the growing mode of density perturbations $D_+(\tau)$,

$$P_{\dot\phi}(k,\tau) = \dot F^2(\tau)P_\phi(k), \quad F(\tau) = D_+(\tau)/a(\tau). \qquad (3.4)$$

For the zero curvature model with a cosmological constant ($\Omega_{m0} + \Omega_{v0} = 1$) one has (Heath 1977)

$$D_+(a) = \frac{\sqrt{\Omega_{m0} + \Omega_{v0}a^3}}{a^{3/2}}\frac{\int_0^a X^{3/2}da}{\int_0^1 X^{3/2}da}, \qquad (3.5)$$

where $X = a/(\Omega_{m0} + \Omega_{v0}a^3)$ and $H_0\tau = \int_0^a da/(\Omega_{m0}a + \Omega_{v0}a^4)^{1/2}$. In a Robertson-Walker universe with no cosmological constant the growth factor is (Heath 1977)

$$D_+(\tau) = -K\frac{3\sin_K(\tau)[\sin_K(\tau) - \tau]}{[\cos_K(\tau) - 1]^2} - 2, \quad a = \frac{\Omega_0}{1 - \Omega_0}\frac{\cos_K(\tau) - 1}{2}, \qquad (3.6)$$

with $\sin_K(\tau)$ and $\cos_K(\tau)$ defined in equations (A.2) and (A.31) (for $K = 0$ the $\sin_K(\tau)$ and $\cos_K(\tau)$ term need to be Taylor expanded to the lowest nonvanishing order).

In a flat $\Omega_{m0} = 1$ universe $D_+(\tau) \propto a(\tau)$ and $P_{\dot\phi}(k)$ vanishes in the linear regime. In this case the lowest order contribution arises from the second order contribution. In second order perturbation theory one expands the density into $\delta = a\delta_1 + a^2\delta_2$. This gives

$$\dot\phi = -\frac{3}{2}\frac{H_0^2}{k^2}\dot a\delta_2. \qquad (3.7)$$

The power spectrum of δ_2 was given by several authors (Peebles 1980; Martínez-González, Sanz & Silk 1992; notation of the paper by Jain & Bertschinger 1994 is

used below),

$$P_{22}(k) = \int d^3q P_\delta(q) P_\delta(|\vec{k} - \vec{q}|) F_2^2(\vec{q}, \vec{k} - \vec{q}), \tag{3.8}$$

$$F_2(\vec{k_1}, \vec{k_2}) = \frac{5}{7} + \frac{2}{7} \left(\frac{\vec{k_1} \cdot \vec{k_2}}{k_1^2 k_2^2} \right) + \frac{\vec{k_1} \cdot \vec{k_2}}{2} \left(\frac{1}{k_1^2} + \frac{1}{k_2^2} \right), \tag{3.9}$$

where $P_\delta(k)$ is the linear density power spectrum. The power spectrum of the potential time derivative is then $P_{\dot\phi} = 9/4 (H_0/k)^4 \dot{a}^2 P_{22}$.

In the fully nonlinear regime even the second-order perturbation theory breaks down and the behavior of the power spectrum $P_{\dot\phi}(k, \tau)$ as a function of time becomes more complicated. It can only be calculated using numerical N-body simulations. An output from an N-body simulation consists of the positions and velocities of the particles in the simulation box. From this one can calculate the density field $\delta(\vec{r}) = \rho/\bar{\rho} - 1$ and momentum density field $\vec{p}(\vec{r}) = (1 + \delta)\vec{v}$ on a fixed grid in the box by counting the number of particles and their velocities near each grid point. Fourier transformation of these quantities gives $\delta(\vec{k})$ and $\vec{p}(\vec{k})$; for simplicity I will drop their explicit k-dependence in the following. Taking the time derivative of the Poisson equation (3.3) and using the continuity equation

$$\dot{\delta} + i\vec{k} \cdot \vec{p} = 0, \tag{3.10}$$

one obtains the following expression

$$\dot{\phi} = \frac{3}{2} \left(\frac{H_0}{k} \right)^2 \Omega_{m0} a^{-1} (\eta \delta + i\vec{k} \cdot \vec{p}), \tag{3.11}$$

with $\eta \equiv \dot{a}/a$. This relation connects the potential time derivative to the density and momentum density. It can also be derived from the second of Einstein's equations (A.11). By averaging over all different modes with the same amplitude k one obtains the power spectrum $P_{\dot\phi}$.

While N-body simulations in principle provide exact information on the evolution of potential for a given model, in practice they are limited by the finite size of the

39

box and the finite resolution. Because there is no power present on scales larger than the size of the simulation box, N-body simulations neglect the nonlinear coupling of these scales to smaller scales. This is particularly important for scales just below the box size, where this coupling is most important. One can test the importance of this effect by comparing the N-body results to the second-order perturbation theory. This provides a useful check of N-body simulations in the weakly nonlinear regime and it allows to extend the results to scales larger than the size of the box in the N-body simulation, as these are the scales where the perturbation theory should be valid. On small scales the N-body simulations are limited by their resolution and this ultimately limits the angular resolution that can be achieved with a given simulation. Both large and small scale cut-offs are investigated in detail in the next section.

An example of various power spectra computed from a high-resolution standard CDM simulation (Gelb & Bertschinger 1994) is shown in Figure (3-1). The spectra have been calculated at high enough redshift ($z = 4$) to be still in the linear regime for the long wavelengths and are multiplied by $4\pi k^3$ to obtain a dimensionless quantity. Dotted line and long-dashed line show the power spectrum of δ and $i\eta^{-1}\vec{k} \cdot \vec{p}$, respectively. The two spectra agree on large scales, where linear theory is a good approximation and makes $\delta \approx -i\eta^{-1}\vec{k} \cdot \vec{p}$. On smaller scales they start to deviate from one another with divergence of momentum density having more power than the density on the same scale. The time derivative of potential $\dot{\phi}$ is proportional to the sum of the two quantities (equation 3.7) and its power spectrum is given by the solid line in Figure (3-1). It starts much lower than the density power spectrum, but eventually rises above it and becomes dominated by the divergence of momentum density. This shows that it is the motion of matter that makes a dominant contribution to $\dot{\phi}$ in the nonlinear regime. The short-dashed line shows the corresponding results from the second-order perturbation theory calculation. On large scales the two spectra agree well, except at the longest wavelength bin, where the disagreement is caused both by insuficient sampling of the largest mode and possibly by the absence of long-wavelength coupling in the N-body simulation. On smaller scales the N-body simulation power spectrum rises above the corresponding second-order per-

turbation case and leads to an increase in the RS effect compared to the second order calculation.

Another approach used in the literature is to approximate the evolution of $\dot{\phi}$ using only the evolution of density (or potential) power spectrum (Martínez-González, Sanz & Silk 1994). For example, one could use semi-analytic approximations by Hamilton et al. (1991), which model the evolution of potential power spectrum, and then try to deduce the power spectrum of $\dot{\phi}$ using $P_{\dot{\phi}} = (d(P_\phi)^{1/2}/d\tau)^2$. This approximation assumes that for a given mode only its amplitude is changing with time, while its phase remains constant and is equivalent to the approximation used by Martínez-González et al. (1994). It gives the correct result in the linear regime, but breaks down in the nonlinear regime. This spectrum is shown with dashed-dotted curve in Figure (3-1), from which one can see that it is a poor approximation both in the perturbative and in the strongly nonlinear regime. The density power spectrum in the second order perturbation theory receives contributions both from $\langle \delta_2 \delta_2 \rangle$ and from $\langle \delta_1 \delta_3 \rangle$, where δ_3 is the third order density perurbation. The two contributions are of the same magnitude and partially cancel each other (Jain & Bertschinger 1994), leading to a severe underestimation of $P_{\dot{\phi}}$ using the above approximation. In the strongly nonlinear regime the power spectrum of $\dot{\phi}$ is dominated by the momentum density, which is determined by the momentum part of single particle phase space. Its evolution is different from the density field evolution, which is determined by the positions of particles. For a proper description of $P_{\dot{\phi}}$ one needs to specify the full particle phase space information, given by both the density and the momentum density fields.

The agreement between the results of the N-body simulation and second-order perturbation theory as a function of expansion factor a is studied in Figure (3-2). The second-order power spectrum grows as a^4 and at late times it eventually rises above the N-body spectrum for small k. On smaller scales the N-body spectrum dominates over the second-order power spectrum. For $k < 1h$ Mpc^{-1} there is a qualitative agreement between the two predictions, which gives confidence that one may use the results from the second order perturbation calculation on scales larger than the size of

simulation box. The discrepancy present at late times even at the longest wavelengths in the simulation could be caused either by the nonlinear effects beyond the second order or by the absence of long-wavelenth coupling in the simulation. It leads to some uncertainty in the final results, which are discussed in the next section.

In the nonlinear stages of evolution there is another Rees-Sciama contribution to CMB anisotropies, associated with the creation of vector metric perturbations. The effect on CMB is described by the time component of the geodesic equation (A.5), $\Delta_\gamma(\vec{n}) = \int_{\tau_{rec}}^{\tau_0} \vec{n} \cdot \dot{\vec{w}} d\tau$. The source for vector modes is the transverse momentum density $\rho \vec{v}_\perp$, as given by the third of Einstein's equations (A.11). In the nonlinear regime it is suppressed by v/c compared to the scalar potential, which has density ρ as a source. In the perturbative regime a more careful comparison is needed, because both contributions vanish in the lowest order. An estimate of the vector amplitude can be obtained by taking the time derivative of the third Einstein's equation and using the continuity equation (A.12) for $\rho \vec{v}$. This gives $\dot{w} \propto k\phi^2$, which has to be compared to $\dot{\phi} \propto k^2 H_0 \phi^2$ from equation (3.7) (with $\delta_2 \propto \delta_1^2$) for the scalar contribution. The vector contribution is thus suppressed by $(kH_0)^{-1} \ll 1$ relative to the scalar contribution and may safely be neglected as a source of CMB anisotropy both in the perturbative and in the strongly nonlinear regime.

3.2 CMB Angular Power Spectrum of the Rees-Sciama Effect

The N-body results were obtained from a particle-particle/particle-mesh simulation of a standard CDM model (Gelb & Bertschinger 1994). It is a $(50h^{-1}\text{Mpc})^3$ simulation with 144^3 particles and a resolution of $32h^{-1}\text{kpc}$, normalized to linear $\sigma_8 = 1$ today (i.e. the linear mass overdensity averaged over spheres of radius $8h^{-1}\text{Mpc}$ is unity today). The power spectrum of $\dot{\phi}$ was calculated on a 384^3 grid. This is about a factor of 4 below the dynamical range of simulation and was chosen because of the computer memory requirements. No shot-noise subtraction was applied to the results

and for this reason only the lower half of k-modes were used in the actual analysis. The largest mode in the simulation was excluded because of insufficient sampling and/or large-scale cutoff problems. This resulted in the dynamic range of N-body simulation between 0.27 and $25h\text{Mpc}^{-1}$ in k. For $k < 0.27h\text{Mpc}^{-1}$ and $z > 9$ the second order perturbation theory calculation was used.

One advantage of the approach presented here is that one can change the parameters of the CDM model without having to use a different simulation or even to recalculate the power spectra of $\dot{\phi}$. For example, a change in the normalization amplitude σ_8 corresponds to a change in the expansion factor and N-body results at expansion factor a can be used as N-body results today for a different CDM model with $\sigma_8 = a$. Similarly we can also rescale the length, which corresponds to a simultaneous change in the shape and the amplitude of the CDM power spectrum. To create a CDM model with $\Omega_{m0}h = 0.25$, which is the model that agrees best with recent large-scale structure surveys (e.g. Peacock & Dodds 1994; da Costa et al. 1994), one needs to rescale the distance by a factor of 2 and instead of the $50h^{-1}$ Mpc box the size of the simulation becomes $100h^{-1}$ Mpc. At the same time the normalization also changes, because $8h^{-1}\text{Mpc}$ scale corresponds to a twice smaller scale in the box, which has more power than the original $8h^{-1}\text{Mpc}$ scale. In such a model the output at $a = 0.61$ corresponds to today if $\sigma_8 = 1$. If one adopts $\sigma_8 = 0.6$ as suggested by cluster abundances (White, Efstathiou & Frenk 1993), then today corresponds to $a = 0.36$ in the original simulation.

Figure (3-4) shows the C_l's for various CDM models discussed above. In all cases the prediction for $\Delta T/T$ is between 10^{-7} and 10^{-6} over a large range of l, which is at least an order of magnitude below the predictions from the primary anisotropies in standard recombination CMB models. For the standard CDM model the power spectrum obtained using only the second order calculation is also plotted. It agrees with the full calculation on large scales, overestimates slightly the C_l's at intermediate scales ($300 < l < 3000$) and underestimates at high l, where strongly nonlinear effects become dominant. In the regime where primary anisotropies are important ($l < 1000$), the second order calculation gives reliable results and may

even overestimate the anisotropies, contrary to previous estimates that it significantly underestimates the anisotropies (Martínez-González et al. 1994).

The RS anisotropies are sensitive to the normalization and shape of the power spectrum. To the extend that the second order theory is valid the amplitude scaling is given by σ_8^4 and so a change of σ_8 by a factor of 2 leads to more than an order of magnitude effect[1] in C_l's. For a given σ_8 a decrease in $\Omega_{m0}h$ gives more large scale power and the Rees-Sciama effect increases on large angular scales. In the models studied here the Rees-Sciama effect becomes significant in comparison with the primary anisotropies only around $l \approx 5000$.

Lack of N-body data on large and small scales leads to some uncertainty in the angular power spectrum. One can see from Figure (3-2) that at late times there is some discrepancy between the second order calculation and N-body results even at the longest wavelengths and the extrapolation to the wavelengths larger than the box is somewhat uncertain. This is studied in Figure (3-3), where the logarithmic contribution to C_l's as a function of wavenumber k (Figure 3-3a) and redshift z (Figure 3-3b) is shown for several values of l. For low l there is a discontinuity at $k = 0.27 h \mathrm{Mpc}^{-1}$ caused by a poor matching of the two power spectra at late times. This discontinuity is larger at low l, where the dominant contribution comes from the wavelengths around the box size at late epochs ($z < 1$). The uncertainty in C_l because of this is at most 20-30% for $l \approx 100$ and is significantly smaller at large l. For small angles where nonlinear effects are dominant one must use the results of N-body simulations to obtain accurate results even at early times. Because for $z > 9$ only second order results are used this causes another discontinuity, which can be seen in Figure (3-3) at $l = 3000$. This effect is less important and leads to a few percent error. In principle the integral in equation (3.2) should be performed from the observer to the last-scattering surface, however due to the finite resolution (small scale cut-off) in the N-body simulation one can only start to integrate from $r = l/k_{max}$, where

---

[1] When comparing the RS effect to the primary anisotropies it is customary to normalize the primary contribution to COBE, which does not change with σ_8. Normalizing it to σ_8 the ratio between the two spectra scales as σ_8^2.

in the present case $k_{max} = 25h\text{Mpc}^{-1}$. For low l this results in a few Mpc cutoff in r, rising up to $400h^{-1}$ Mpc at $l = 10^4$. At this value of l the dominant scale is $k \approx 5h\text{Mpc}^{-1}$ (Figure 3-3a) and the scales with $k > 25h\text{Mpc}^{-1}$ still have a relatively small contribution. Only for $l \gg 10^4$ the scales smaller than $(25h)^{-1}\text{Mpc}$ become significant and limit the dynamic range of angular power spectrum.

The redshift distribution studied in Figure (3-3b) indicates that the typical contribution to the RS effect comes from z around 1 at $l > 1000$. At lower l the dominant contribution comes from redshifts below 1 (e.g. $z \approx 0.2$ at $l \approx 100$), but is never dominated by very nearby structures. This is comforting as it guarantees that the fair sampling criterion is satisfied. Moreover, the observational bias caused by observing areas of the sky which do not contain large nearby clusters should be small for all but the lowest values of l.

The conclusion derived from above is that in the models with no early reionization the Rees-Sciama effect is negligible compared to the primary anisotropies over most of observationally interesting scales ($\theta > 2'$) and is in any case below the present-day observational limits ($\sim 10^{-6}$ in $\Delta T/T$) on all angular scales. While the results presented here are specific to the flat CDM models, other models that reproduce the observed cluster abundance and large-scale correlations should give comparable results. The main additional effect present in the models with $\Omega_{m0} < 1$ is the decay of potential on linear scales (equations 3.2-3.6), which gives an important additional linear contribution to the CMB anisotropies on very large scales (Kofman & Starobinski 1985; Kamionkowski & Spergel 1994) and also on smaller scales in reionized models (Hu & Sugiyama 1994). The nonlinear RS effect itself is actually smaller in low Ω_{m0} models because for a given density normalization both the potential and the velocity decrease with Ω_{m0} and lead to a smaller $\dot{\phi}$ (this will be partially offset by the longer comoving radial pathlength). The linear RS effect is also present in mixed or hot dark matter models, where massive neutrinos contribute to the dark matter and their free-streaming causes the potential to change in time at late epochs. This leads to a small, but potentially measurable effect on primary CMB anisotropies (e.g. Ma & Bertschinger 1995). If the universe was reionized early enough so that it became

45

optically thick, then the primary anisotropies would have been erased and the RS effect would dominate over the primary contribution at a much lower l. However, in this case secondary anisotropies caused by the Vishniac effect would also be more important and would swamp the RS effect, as they give few times 10^{-6} contribution in the models studied here (e.g. Persi et al. 1995). Therefore the RS effect is likely to be unimportant in our universe on arcminute scales and above regardless of the particular model of structure formation or of its reionization history.

Bibliography

[1] Bode, P., & Bertschinger, E. 1995, preprint astro-ph 9504040

[2] da Costa, L. N., Vogeley, M. S., Geller, M. J., Huchra, J. P., & Park, C. 1994, ApJ437, L1

[3] Gelb, J., & Bertschinger, E. 1994, ApJ, 436, 467

[4] Hamilton, A. J. S., Kumar, P., Lu, E., & Matthews, A. 1991, ApJ, 374, L1

[5] Heath, D. J., 1977, MNRAS, 179, 351

[6] Hu, W., & Sugiyama, N. 1994, Phys. Rev. D, 50, 627

[7] Jain, B., & Bertschinger, E., 1994, ApJ, 431, 495

[8] Kamionkowski, M. & Spergel, D. N. 1994, ApJ, 432, 7

[9] Kofman, L., & Starobinsky, A. 1985, Sov. Astron. Lett., 11, 271

[10] Ma, C. P., & Bertschinger, E. 1995, ApJ, to be published

[11] Martínez-González, E., Sanz, J. L., & Silk, J. 1992, Phys. Rev. D, 46, 4196

[12] Martínez-González, E., Sanz, J. L., & Silk, J. 1994, ApJ, 436, 1

[13] Mollerach, S., Gangui, A., Lucchin, F., & Matarrese, S. 1995, preprint

[14] Munshi, D., Souradeep, T., & Starobinski, A. A. 1994, preprint IUCAA-38/94

[15] Peacock, J. A., & Dodds, S. J. 1994, MNRAS, 267, 1020

[16] Peebles, P. J. E., The Large Scale Structure of the Universe (Princeton University, Princeton, NJ, 1980)

[17] Persi, F. M., Spergel, D. N., Cen, R., & Ostriker, J. P. 1995, ApJ, 442, 1

[18] Rees, M. J., & Sciama, D. W. 1968, Nature, 517, 611

[19] Tuluie, R., & Laguna, P. 1995, submitted to ApJ

[20] White, S. D. M., Efstathiou, G., & Frenk C. S. 1993, MNRAS, 262, 1023
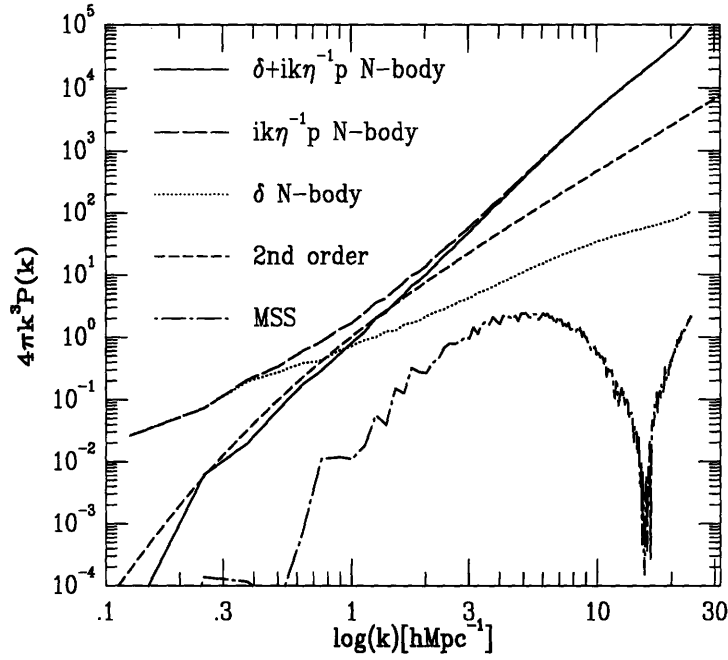
Figure 3-1: Comparison between various power spectra discussed in the text at $z = 4$. MSS denotes the Martínez-Gonzalez et al. (1994) approximation using the evolution of the density power spectrum alone. The curve was computed by finite differencing of two power spectra at different times and is noisier than other spectra, which are computed at the same time.
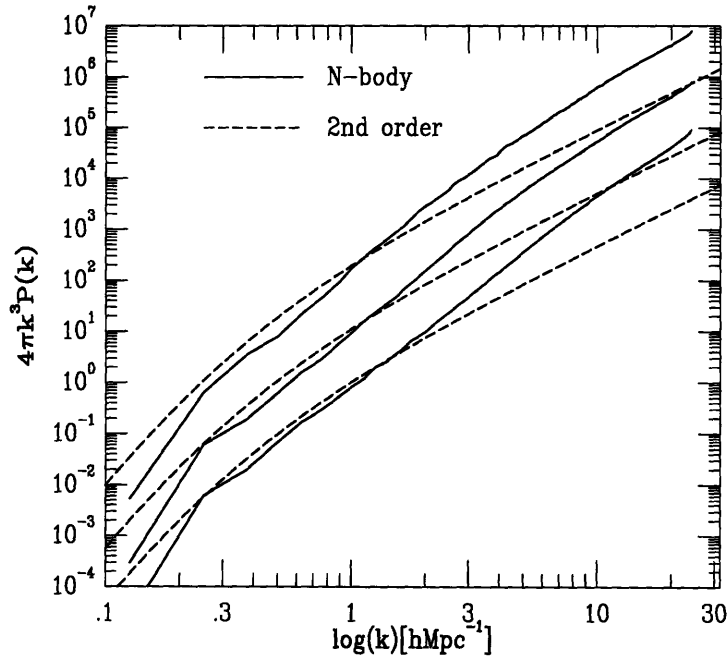
Figure 3-2: Comparison between N-body and second order calculations of $\delta + i\eta^{-1}\vec{k}\cdot\vec{p}$ as a function of expansion factor $a = (1+z)^{-1}$. From bottom to top the three spectra are for $a = 0.2$, $a = 0.4$ and $a = 0.8$, respectively.

49
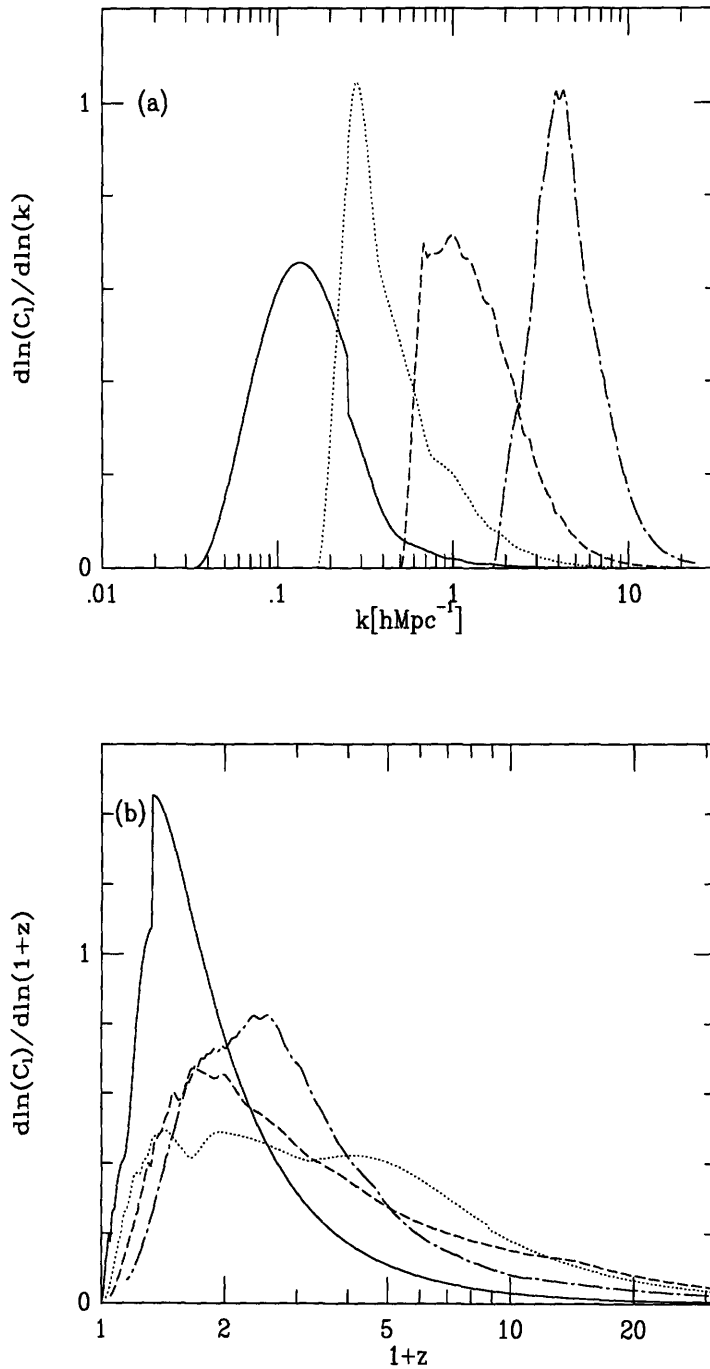
Figure 3-3: Logarithmic contribution to C_l as a function of wavenumber k (a) for the standard CDM model. From left to right the l values are: 300, 1000, 3000 and 10000. In (b) the corresponding logarithmic contribution to C_l as a function of redshift z is plotted.

50
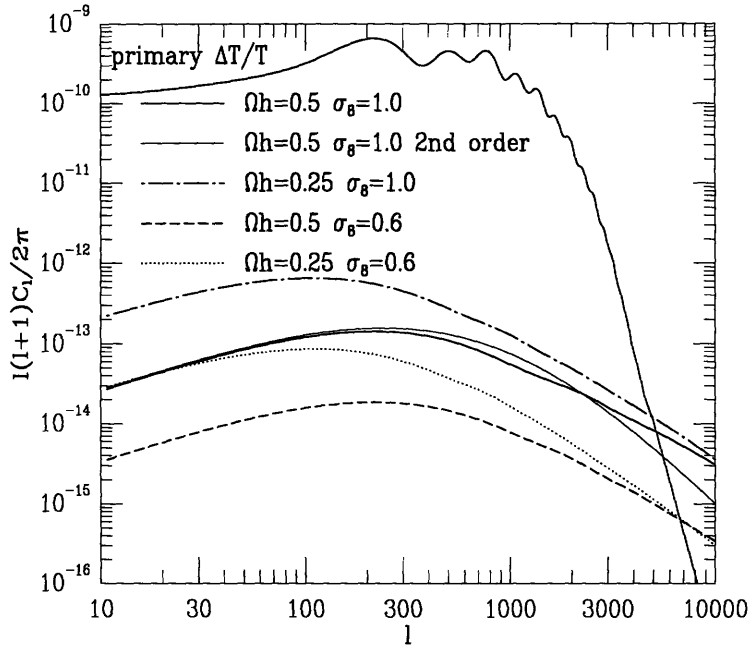
Figure 3-4: RS contribution to the angular power spectra $l(l+1)C_l/2\pi$ for various CDM models. Also plotted is the RS effect for the standard CDM case from the second order calculation and the primary contribution to the spectrum for a COBE normalized adiabatic CDM model ($h = 0.5$, $\Omega_{b0}h^2 = 0.05$), adopted from Bode & Bertschinger (1995).

Chapter 4

Large Scale Structure Effects on the Gravitational Lens Image Positions and Time Delay

In this Chapter[1] I investigate the effect of weak lensing on observable properties of strong gravitational lenses, in particular, the relative positions and time delays between images of a single lensed source. The main goal of this investigation is to estimate whether large-scale structure importantly changes the properties deduced from strong lens analysis in the thin-lens approximation without the large-scale structure. For simplicity I restrict the calculations in this chapter to linear theory in flat space. A more general treatment is presented in Appendix B and Chapter 5.

4.1 Fluctuations in Angular Position

The first question one would like to answer is what is the rms fluctuation in the photon direction at the observer's position relative to the unperturbed direction, given by

$$\sigma_\gamma = \langle \delta\vec{\gamma}(0, r_{OS}) \cdot \delta\vec{\gamma}(0, r_{OS}) \rangle^{1/2}, \tag{4.1}$$

---

where $\delta\vec{\gamma}(0, r_{OS})$ is the difference between the photon direction at the source position (given by the radial distance $\chi_S \equiv r_{OS}$) and its observed direction at $r = 0$ and is computed by adding all the deflections along the photon trajectory,

$$\delta\vec{\gamma}(0, r_{OS}) = -2 \int_0^{r_{OS}} \vec{\nabla}_\perp \phi \, dr. \tag{4.2}$$

The variance σ_γ can be calculated from the correlation function as given in equation (B.13) with $\theta = 0$ and $W(r, r_{OS}) = 1$. Assuming linear evolution and no cosmological constant one obtains

$$\sigma_\gamma = \left(16\pi^2 r_{OS} \int_0^\infty P_\phi(k) k^3 dk \right)^{1/2}, \tag{4.3}$$

where P_ϕ is the power spectrum of the potential today. The rms fluctuation in photon direction at the distance r_{OS} from the source, σ_γ, is related to the rms angular fluctuation of the true source position relative to the observed position, $\sigma_\theta = \langle \delta\vec{\theta} \cdot \delta\vec{\theta} \rangle$, where $\delta\vec{\theta}$ is defined in equation (B.8). From equation (B.13) with $\theta = 0$ one finds

$$\sigma_\theta = \frac{\sigma_\gamma}{\sqrt{3}} = \left(\frac{16\pi^2 r_{OS}}{3} \int_0^\infty P_\phi(k) k^3 dk \right)^{1/2}. \tag{4.4}$$

To get some intuition about the scaling of the amplitude with the parameters I will present an estimate of the fluctuations for a particularly simple power spectrum approximating the scale-invariant Peebles-Harrison-Zel'dovich spectrum with a physical transfer function:

$$P_\phi(k) = \begin{cases} A k^{-3} & , k < k_0 \\ A k^{-7} k_0^4 & , k > k_0 \end{cases} \tag{4.5}$$

The spectral indices have been chosen to agree with the cold dark matter model in the limits of small and large k. A particularly convenient normalization of $P_\phi(k)$ is given by the cosmic microwave background anisotropy measured by $COBE$: the quadrupole $Q_2 = (\Delta T/T)_2 = (7 \pm 1) \times 10^{-6}$ (Górski et al. 1994). On the large scales probed by $COBE$ the dominant contribution to $\Delta T/T$ is given by the Sachs-Wolfe (1967) effect,

53

induced by the same metric fluctuations that cause the fluctuations in time delay and image positions. Assuming no tensor mode contribution to CMB anisotropies and isentropic (adiabatic) fluctuations one can express the quadrupole in terms of the power spectrum of the potential (Bond & Efsthathiou 1987) as

$$Q_2^2 = \frac{20\pi K_2^2}{9} \int_0^\infty k^2 P_\phi(k) j_2^2(2k/H_0) dk. \qquad (4.6)$$

Here $j_2(x)$ is the spherical Bessel function of order 2 and $K_2^2 \geq 1$ is the amplification coefficient due to the time dependent potential (Kofman & Starobinsky 1985). If $\Omega_{m0} = 1$ the potential is time independent and $K_2^2 = 1$. For the power spectrum defined in equation (4.5) one gets

$$Q_2^2 = \frac{5\pi K_2^2 A}{27}. \qquad (4.7)$$

Applying this power spectrum to equations (4.3) and (4.4) I find

$$\sigma_\theta = \frac{\sigma_\gamma}{\sqrt{3}} \approx 10 Q_2 (k_0 r_{OS})^{1/2}. \qquad (4.8)$$

This result has a simple physical interpretation. For power spectra like in equation (4.5) the dominant contribution to gravitational deflection of light comes from the scales near the turnover position k_0^{-1}. A photon travelling through a coherent structure of size k_0^{-1} will be deflected by $\delta\gamma \approx 2\phi \approx 6Q_2$, where the last relation assumes ϕ is scale invariant for $k < k_0$ and is therefore fixed by the Sachs-Wolfe effect on the Hubble distance scale. Each region of size k_0^{-1} makes an independent contribution to the deflection. Since the individual contributions are random, the photon exhibits a random walk with $\sigma_\gamma \approx N^{1/2}\delta\gamma$, where $N = k_0 r_{OS}$. Numerical factors aside this agrees with equation (4.8). A reasonable value for the turnover position in the power spectrum is given by $k_0^{-1} = 10$ Mpc. Taking $r_{OS} = 1$ Gpc as a typical source distance I find $\sigma_\gamma \approx 3 \times 10^{-4} (k_0 r_{OS}/100)^{1/2} \approx 1'(k_0 r_{OS}/100)^{1/2}$. This is small compared to 1, which justifies the small deflection angle assumption. It also verifies that the pathlengths are not significantly lengthened by the perturbations.

Note that the fluctuations in the angular position σ_θ are of the order of arcminutes (see also Linder 1990), which means that the true positions of distant objects in the universe, such as quasars, differ from the measured photon directions at the observer on average (rms) by this amount. These fluctuations arise already because of the linear structures (voids and superclusters) and are present even when there are no nonlinear objects (like galaxies and clusters) intersecting the photon trajectories. The fluctuations are much larger than a typical image separation in a lens system, which is of the order of a few arcseconds. The large total deflections are not directly observable in a single lens system, because only the relative positions of images can be measured. Figure (4-1) shows photon propagation in a typical two-image GL system. Despite the fact that the deflection of any single photon ray can be large, the lens equation will still give the same solution as in the unperturbed case, provided that large-scale structure (LSS) deflects the two photons approximately by the same amount. This will be examined below. Although the deflection of a photon ray relative to the unperturbed direction is not directly observable from the positions, one might worry that it could produce significant time delay fluctuations. I will address this question in the next section.

LSS effects on the relative image positions are given by $\sigma_{\Delta\gamma}$ and $\sigma_{\Delta\theta}$, the dispersions in the relative direction and in the relative angular position separation between two image rays. I will denote the two rays with A and B, separated in direction at the observer's position by an angle $\vec{\theta} = \vec{\theta}^A - \vec{\theta}^B$. The potential can be divided into a stochastic part, which describes the LSS, and a non-stochastic part describing the primary lensing object and I assume there are no correlations between these two parts.

The difference between the two direction vectors caused by LSS between the lens (at radial distance r_{OL}) and the observer is given by

$$\Delta\vec{\gamma}(r_{OL}) = \vec{\theta} + \delta\vec{\gamma}^A(0, r_{OL}) - \delta\vec{\gamma}^B(0, r_{OL}), \qquad (4.9)$$

where $\delta\vec{\gamma}^A(0, r_{OL})$ and $\delta\vec{\gamma}^B(0, r_{OL})$ are the deflections caused by LSS for the rays A

and B, respectively. I excluded the non-stochastic deflection from the primary lens itself. For a fixed separation between the two photons at the observer's position θ, the rms fluctuation in the angle between the two rays at the lens position is given by

$$\sigma_{\Delta\gamma}(\theta) = \langle\left[\delta\vec{\gamma}^A(0, r_{OL}) - \delta\vec{\gamma}^B(0, r_{OL})\right]^2\rangle^{1/2},$$ (4.10)

where the dispersion can be calculated from the correlation function from equation (B.13) with $W(r, r_{OL}) = 1$. Assuming for simplicity that the scales contributing to the fluctuations are much larger than the typical separation between the two rays one can Taylor expand the Bessel function J_0 and obtain

$$\sigma_{\Delta\gamma} = 2\pi\theta\left[\frac{r_{OL}^3}{3}\int_0^\infty P_\phi(k)k^5 dk\right]^{1/2}.$$ (4.11)

Replacing θ with $(r_{OL}/r_{LS})\theta$ and r_{OL} with r_{LS} (where r_{LS} is the source-lens distance) in equation (4.11) gives the rms fluctuation between the two ray directions accumulated between the source and the lens. Adding the two contributions in quadrature gives the rms fluctuation accumulated between the source and the observer, neglecting the correlations between paths on either side of the lens. The dispersion of the angular position between two rays in the lens plane $\sigma_{\Delta\theta}$ is defined in equation (B.20). It can be calculated from equation (B.13) by setting $W(r, r_{OL}) = (1 - r/r_{OL})$, which under the same approximation as above gives for the contribution between the observer and the lens,

$$\sigma_{\Delta\theta} = \frac{\sigma_{\Delta\gamma}}{\sqrt{10}} = 2\pi\theta\left(\frac{r_{OL}^3}{15}\int_0^\infty P_\phi(k)k^5 dk\right)^{1/2}.$$ (4.12)

For the simple power spectrum of equation (4.5) I find

$$\sigma_{\Delta\gamma} = \sqrt{10}\sigma_{\Delta\theta} \approx 6Q_2(k_0 r_{OL})^{3/2}\theta \approx 0.025(k_0 r_{OL}/100)^{3/2}\theta.$$ (4.13)

Again, there is a simple physical explanation of this result. Two photons separated by an angle θ sample different potentials, $\delta\phi \approx (\nabla_\perp\phi)r\theta \approx k_0\phi r\theta$, including only the peak power contribution around k_0. The separation $r\theta$ is largest at the lens, but

56

only falls to one-half for distances half and three-halves as far, so it is a reasonable approximation to fix r to r_{OL}. A coherent structure of size k_0^{-1} leads to an angular difference of $\delta\gamma \approx 2\delta\phi$ and there are $N = k_0 r_{OL}$ random and independent contributions. The total angular difference is just an incoherent sum of individual contributions, $\sigma_{\Delta\gamma} \approx N^{1/2}\delta\gamma$, which, numerical factors aside, reproduces equation (4.13).

A more direct way to estimate the amplitude of image position fluctuations is to use the observations of correlated distortions of distant galaxy images. This can be described by the ellipticity correlation function $C_{pp}(\theta)$ (Blandford et al. 1991, Appendix B), which describes the correlations in the ellipticities of galaxy images as a function of angular separation θ. The ellipticity correlation function at zero lag, $C_{pp}(0)$, can be related to the power spectrum using the equation (B.14)

$$C_{pp}(0) = \frac{16\pi^2 r_g^3}{30} \int_0^\infty P_\phi(k) k^5 dk, \qquad (4.14)$$

where I assumed for simplicity that all the galaxies lie at the same distance r_g (Kaiser 1992; Blandford et al. 1991). From this one sees that

$$\frac{\sigma_{\Delta\theta}}{\theta} = \frac{\sigma_{\Delta\gamma}}{\sqrt{10}\theta} = \left[\frac{C_{pp}(0)}{2}\right]^{1/2} (r_{OL}/r_g)^{3/2}. \qquad (4.15)$$

For most cosmological models and redshifts around $z \approx 1$, the linear theory prediction of equation (4.11) gives $\sigma_{\Delta\theta}/\theta$ of the order of a few percent. This has to be corrected for the nonlinear effects, which are somewhat uncertain. Theoretical estimates (Kaiser 1992; Chapter 5) and N-body simulations (Blandford et al. 1991; Miralda-Escudé 1991) suggest that $C_{pp}(0)$ is unlikely to exceed 10^{-3}. This is also supported by the observational data. Mould et al. (1994) report a detection of a signal with a value $C_{pp}(1' < \gamma < 5') = (5.6 \pm 0.6) \times 10^{-4}$, which, after seeing correction, implies average ellipticity within a few arcminutes radius of about 0.05. Assuming this value one finds $\sigma_{\Delta\theta}/\theta \approx 0.08(r_{OL}/r_g)^{3/2}$, with $r_g \approx 0.6H_0^{-1}$. However, the authors could not exclude the possibility that the observed signal is due to systematic effects. This is also suggested by Fahlman et al. (1994), who report a null detection

of average ellipticity within a 2.76' radius aperture with a sensitivity of about 1.3%, which after adjustment to r_g above implies an upper limit $\sigma_{\Delta\theta}/\theta < 0.03(r_{OL}/r_g)^{3/2}$. These measurements give average ellipticities in typically arcminute size windows and do not probe $C_{pp}(\theta)$ on scales below 1'. Observationally it is difficult to give reliable estimates on smaller scales because one has to distinguish between the signal and the noise from the intrinsic ellipticities of galaxies. A rather weak upper limit on $C_{pp}(0)$ can be obtained simply from the average ellipticity of galaxies, which is of the order of 0.4 and is dominated by intrinsic ellipticities. Despite some uncertainty from the model predictions and observations, it appears unlikely that the relative fluctuations in the image separation angle exceed a level of a few percent for sources at modest redshifts ($z \approx 1$).

The conclusion above justifies the assumption that the rms fluctuation is small compared to the measured image separation. The fact that $\sigma_{\Delta\theta}/\theta \ll 1$ also implies that one cannot have multiple images produced by LSS alone. Therefore, multiple images can only be formed from nonlinear structures, such as galaxies or clusters. This conclusion has previously been obtained using N-body simulations by Jaroszynski et al. (1991) and using semi-analytical methods by Bartelmann & Schneider (1991). The fluctuations in angular image separation, although small, are in most cases larger than the observational errors on the image positions (typically less than 0.01 arcsecond/arcsecond $\sim 10^{-2}$). Therefore, LSS effects are a major source of uncertainty in the image positions. This effect limits our ability to reconstruct the lens potential using the image positions and should be included in the modelling of lens parameters. In the first order the effect is to add additional constant shear in the lens plane. The uncertainty due to LSS is therefore mainly in the shear, whereas the other components of lens reconstruction are less affected by LSS.

In equations above I neglected the correlations between LSS and the primary lens. This is justified because the two are correlated only over a correlation length distance, which is much smaller than the typical pathlength. While there are N uncorrelated regions of size k_0^{-1} along the photon path, only one of those is strongly correlated with the primary lens. The contribution from that region can be regarded as being

part of the primary lens itself. The error due to this approximation is therefore of the order of $N^{-1} = (k_0 r_{OS})^{-1} \ll 1$.

4.2 Fluctuations in Time Delay

In this section I compute the dispersion in time delay between two images. For this purpose it is useful to define the time delay relative to the normal of the lens plane and not relative to the source-observer line. I define the lens plane at the lens redshift z_l to be orthogonal to what would be the source-observer line in the absence of LSS effects (Figure 4-1). Relative to the lens plane normal, the incoming and outgoing photon direction vectors in the lens plane are $\vec{\gamma}^{A,in}$, $\vec{\gamma}^{A,out}$ and $\vec{\gamma}^{B,in}$, $\vec{\gamma}^{B,out}$ for the images A and B, respectively. The difference between the incoming and outgoing photon direction gives the deflection angles in the lens plane, $\vec{\alpha}^A$ and $\vec{\alpha}^B$. These can be obtained by modelling the lens potential using various observational constraints, such as image magnifications, velocity dispersion of the lensing galaxy and/or cluster, positions of other images or arcs, etc.

In the absence of LSS the time delay between two images is given from equations (B.6), (B.7) by

$$
\begin{aligned}
\Delta t &= \frac{1}{2}\left\{ r_{LS}[(\gamma_1^{A,in})^2 - (\gamma_1^{B,in})^2] + r_{OL}[(\gamma_1^{A,out})^2 - (\gamma_1^{B,out})^2] \right\} - 2(\Phi_{lens}^A - \Phi_{lens}^B) \\
&= \frac{r_{OL} r_{OS}}{2 r_{LS}}[(\gamma_1^{A,in})^2 - ((\gamma_1^{B,in})^2] - 2(\Phi_{lens}^A - \Phi_{lens}^B).
\end{aligned}
\tag{4.16}
$$

Here Φ_{lens}^A and Φ_{lens}^B are the integrals of the primary lens potential for the two rays,

$$
\Phi_{lens} = \int_{r_{OL}-\epsilon}^{r_{OL}+\epsilon} \phi(r) dr
\tag{4.17}
$$

with $\epsilon/r_{OL} \ll 1$. Equation (4.16) is the usual time delay expression in the thin lens approximation (e.g. Blandford & Narayan 1986; Blandford & Kochanek 1987; Schneider, Ehlers & Falco 1992). Note that the difference between the two outgoing photon directions gives the observed image splitting.

Adding LSS moves both the source and the observer, for a fixed lens plane (Figure

4-1). The time delay between the two rays is now given by

$$
\begin{aligned}
\Delta t \;=\;& \frac{1}{2} \int_{r_{OL}}^{r_{OS}} \left\{ [\vec{\gamma}^{A,in} - \delta\vec{\gamma}^A(r_{OL}, r)]^2 - [\vec{\gamma}^{B,in} - \delta\vec{\gamma}^B(r_{OL}, r)]^2 \right\} dr \\
+\;& \frac{1}{2} \int_0^{r_{OL}} \left\{ [\vec{\gamma}^{A,out} + \delta\vec{\gamma}^A(r, r_{OL})]^2 - [\vec{\gamma}^{B,out} + \delta\vec{\gamma}^B(r, r_{OL})]^2 \right\} dr \\
-\;& 2 \left\{ \int_{r_{OL}}^{r_{OS}} [\phi^A(r) - \phi^B(r)] dr + \Phi_{lens}^A - \Phi_{lens}^B + \int_0^{r_{OL}} [\phi^A(r) - \phi^B(r)] dr \right\} (4.18)
\end{aligned}
$$

This equation is similar to the time delay defined in equations (B.6) and (B.7), except that here the geometrical contribution is measured relative to the normal of the lens plane. The first two lines in equation (4.18) give the geometrical time delay between the lens and the source and between the lens and the observer, respectively. In the third line I have written the gravitational time delay contribution coming from the potential between the lens and the source, from the primary lens potential and from the potential between the lens and the observer, respectively. The LSS ($\delta\vec{\gamma}$, ϕ) and primary lens ($\vec{\gamma}^{in}$, $\vec{\gamma}^{out}$, Φ_{lens}) contributions are thus explicitly separated.

I will calculate first the time delay contribution between the ray A and the fiducial ray accumulated between the lens and the observer. The fiducial ray is defined to start perpendicular to the lens plane and end at the observer's positions. The total time delay is obtained by adding a similar contribution from the lens to the source and subtracting the same terms for the ray B. The fiducial ray direction is given by

$$
\vec{\gamma}^f(r) = \vec{\delta\gamma}(r, r_{OL}) = -2 \int_r^{r_{OL}} \vec{\nabla}_\perp \phi(r) dr, \tag{4.19}
$$

where $\vec{\nabla}_\perp \phi(r)$ is computed along the fiducial ray. The direction of the ray A is

$$
\vec{\gamma}^A(r) = \vec{\gamma}^f(r) + \vec{\gamma}^{A,out} + \delta\vec{\gamma}^A(r, r_{OL}). \tag{4.20}
$$

Here $\delta\vec{\gamma}^A(r, r_{OL})$ is the difference between the LSS induced ray deflections at r and can be calculated using the Taylor expansion of potential around the fiducial ray. The

image ray position relative to the fiducial ray is

$$\vec{x}_{\perp}^{A}(r) = \vec{x}_{\perp}^{A}(r_{OL}) + \vec{\gamma}^{out,A}(r_{OL} - r) + \int_{r}^{r_{OL}} \delta\vec{\gamma}^{A}(r', r_{OL})dr'. \qquad (4.21)$$

The initial lens plane position of the image ray relative to the fiducial ray, $\vec{x}_{\perp}^{A}(r_{OL})$, is not a free parameter, since it has to satisfy the constraint

$$\vec{x}_{\perp}^{A}(0) = 0. \qquad (4.22)$$

From this I obtain

$$\vec{x}_{\perp}^{A}(r) = -\vec{\gamma}^{out,A}r - \int_{0}^{r} \delta\vec{\gamma}^{A}(r', r_{OL})dr'. \qquad (4.23)$$

The gravitational time delay contribution is obtained from the Taylor expansion of the potential around the fiducial ray,

$$\Delta t_{grav} = \int_{0}^{r_{OL}} \left\{ -2\vec{\nabla}_{\perp}\phi(r) \cdot \vec{x}_{\perp}^{A}(r) + O[(\vec{x}_{\perp}^{A}(r)^{2}] \right\} dr. \qquad (4.24)$$

The geometrical time delay contribution is given by

$$\begin{aligned}
\Delta t_{geom} &= \frac{1}{2}\int_{0}^{r_{OL}} [\vec{\gamma}^{A}(r)^{2} - \vec{\gamma}^{f}(r)^{2}]dr \\
&= \frac{(\vec{\gamma}^{out,A})^{2}r_{OL}}{2} + \int_{0}^{r_{OL}} \left[\vec{\gamma}^{f}(r) \cdot \vec{\gamma}^{out,A} + \vec{\gamma}^{f}(r) \cdot \delta\vec{\gamma}^{A}(r, r_{OL}) \right. \\
&\quad + \left. \vec{\gamma}^{out,A} \cdot \delta\vec{\gamma}^{A}(r, r_{OL}) + \frac{\delta\vec{\gamma}^{A}(r, r_{OL})^{2}}{2} \right] dr. \qquad (4.25)
\end{aligned}$$

Integrating by parts the terms involving $\vec{\gamma}^{f}(r)$ one finds

$$\int_{0}^{r_{OL}} \vec{\gamma}^{f}(r) \cdot [\vec{\gamma}^{out,A} + \delta\vec{\gamma}^{A}(r, r_{OL})]dr =$$
$$\int_{0}^{r_{OL}} \left\{ -2\vec{\nabla}_{\perp}\phi(r) \cdot \int_{0}^{r} [\vec{\gamma}^{out,A} + \delta\vec{\gamma}_{\perp}^{A}(r', r_{OL})]dr' \right\} dr. \qquad (4.26)$$

This is exactly cancelled by the first order term in Δt_{grav} (equation 4.24). Therefore, $\vec{\gamma}^{f}$ completely drops out of the time delay expression and using time delay measurements one cannot infer any information on the absolute deflection angle. This

is quite remarkable, given that separately the geometrical and gravitational LSS induced fluctuations are approximately 15 yr $(k_0 r_{OS}/100)^{1/2}(r_{OS}/1\mathrm{Gpc})(\Delta\gamma_0/1'')$, much larger than the expected time delay from the primary lens itself, of the order of 0.1 yr $(r_{OS}/1\mathrm{Gpc})(\Delta\gamma_0/1'')^2$.

Adding the geometrical and gravitational time delay contributions one finally obtains

$$\Delta t^A = \frac{(\vec{\gamma}^{out,A})^2 r_{OL}}{2} + \int_0^{r_{OL}} [\vec{\gamma}^{out,A} \cdot \delta\vec{\gamma}_\perp^A(r) + \frac{1}{2}\delta\vec{\gamma}_\perp^A(r)^2 + O((\vec{x}_\perp^A(r)^2)]dr. \quad (4.27)$$

The first term in equation (4.27) gives the largest contribution and is the term that one would also have in the absence of LSS (compare with equation 4.16). The second term is smaller than the first term approximately by $\sigma_{\Delta\theta}/\theta$. The last two terms in equation (4.27) are further suppressed by $\sigma_{\Delta\theta}/\theta$ relative to the second term and can be neglected.

What, then, is the LSS induced fluctuation that causes the reconstructed time delay to differ from the true time delay? The observer measures the image separation angle that is almost, but not exactly, given by $\vec{\gamma}^{A,out} - \vec{\gamma}^{B,out}$, so that the reconstructed time delay differs somewhat from equation (4.16). It is not possible to give an exact prediction of the reconstructed time delay without specifying the detailed lens model and taking into account all of the observational constraints. It is clear, however, that the fluctuation in the reconstructed time delay is due only to the fluctuation in the relative angle separation, part of which is described by the second term in equation (4.27). Given that $\sigma_{\Delta\theta}/\theta \ll 1$, the relative effects on the time delay will also be of that order. I conclude that the time delay fluctuation induced by LSS is of the order of $\sigma_{\Delta\theta}/\theta$, which is of the order of a few percent for sources and lenses at cosmological distances.

62

4.3 Conclusions

I investigated the LSS effects on measurable properties of gravitational lens systems, in particular on the image positions and time delays. The method based on a geodesic equation in a weakly perturbed flat Robertson-Walker metric is valid for a general matter distribution between the source and the observer. The advantage of this approach compared to previous work on this subject is that it only assumes the knowledge of evolution of density power spectrum, which can easily be related to other measurements of LSS to obtain quantitative predictions. The same approach can also be used to investigate light propagation in a non-flat universe (Appendix B) and the conclusions in this paper do not significantly depend on the assumed value of Ω_0. The rms fluctuation in the relative positions of images is $\sigma_{\Delta\theta}/\theta \sim 0.025(k_0 r_{OL}/100)^{3/2}$, for a LSS density power spectrum peaking at wavelength k_0. For most realistic models of LSS this is much smaller than unity and so one does not expect multiple images generated from LSS. Nevertheless, these fluctuations are likely to be larger than the observational errors and should be included in the modelling of lens parameters. Similarly, rms fluctuation in time delay due to LSS are caused only by the uncertainties in the relative image positions and are also approximately given by $0.025(k_0 r_0/100)^{3/2}$ and LSS does not significantly affect the time delays. While the same method can be used to predict fluctuations in the relative image magnification and orientation, a simple estimate shows that the effect on these observables is negligible. The rms fluctuation in relative magnification between two images $\Delta M/M$ is given approximately by $\Delta M/M \sim (\nabla_\perp M) r_{OS} \Delta\gamma_0/M \sim (k_0 r_{OS} \Delta\gamma_0) C_{pp}(0)^{1/2} \sim 10^{-5}$, well below the measurement errors.

If LSS does not induce significant time delay fluctuations, then this would remove one of the major objections against using time delay measurements to determine H_0. Significant problems related to the robustness of the lens reconstructions still remain and are preventing the method at present from giving a reliable estimate of H_0 (see e.g. Bernstein, Tyson & Kochanek 1993 for a discussion of lens reconstruction in 0957+561). Moreover, the above analysis does not exclude the possibility that a ho-

mogeneous sheet of matter is present in the lens plane, because in our treatment this sheet of matter is part of the primary lens. A uniform matter distribution, which is likely to be overdense close to the primary lens, cannot be determined from the image positions, but it does affect the length scale and makes the deduced value of Hubble constant larger than the true value (Borgeest & Refsdal 1984; Falco, Gorenstein & Shapiro 1991). To solve this problem one must either use dynamical estimates of lens mass (by measuring velocity dispersion of the galaxy, Rhee 1991) or measure the magnification of background galaxies because of this additional mass sheet (Bartelmann & Narayan 1995). Although severe, these problems are not unsolvable and GL time delay method remains one of the few methods that can provide information on the global distance scale and geometry of the universe.

Bibliography

[1] Bartelmann, M. & Narayan, R. 1995, CfA preprint

[2] Bartelmann, M. & Schneider, P. 1991, A&A, 248, 349

[3] Bernstein, G. M., Tyson, J. A., & Kochanek, C. S. 1993, AJ, 105, 816

[4] Blandford, R. D., & Narayan, R. 1986, ApJ, 310, 568

[5] Blandford, R. D., & Kochanek, C. S. 1987, in: Dark Matter in the Universe, eds. Bahcall, J., Piran, T., & Weinberg, S. (World Scientific: Singapore)

[6] Blandford, R. D., Saust, A. B., Brainerd, T. G., & Villumsen, J. V. 1991, MNRAS, 251, 600

[7] Bond, J.R., & Efsthathiou, G. 1987, MNRAS, 226, 665

[8] Borgeest, U., & Refsdal, S. 1984, A&A, 141, 318

[9] Górski K. M. et al. 1994, ApJ, 430, L89

[10] Jaroszynski, M., Park, C., Paczynski, B., & Gott, J., R., III 1991, ApJ, 365, 22

[11] Kaiser, N. 1992, ApJ, 388, 272

[12] Fahlman, G. G., Kaiser, N., Squires, G. & Woods, D. 1994, ApJ, 437, 56

[13] Kofman, L., & Starobinsky, A. 1985, Sov. Astron. Lett., 11, 271

[14] Linder, V. E. 1990, MNRAS, 243, 362

[15] Miralda-Escudé, J. 1991, ApJ, 380, 1

[16] Mould, J., Blandford, R., Villumsen, J., Brainerd, T., Smail, I., Small, T., & Kells, W. 1994, preprint

[17] Rhee, G. 1991, Nature, 350, 211

[18] Sachs, R. K., & Wolfe, A. M. 1967, ApJ, 147, 73

[19] Schneider, P., Ehlers, J., & Falco, E. E. 1992, Gravitational Lenses (Springer-Verlag: New York)
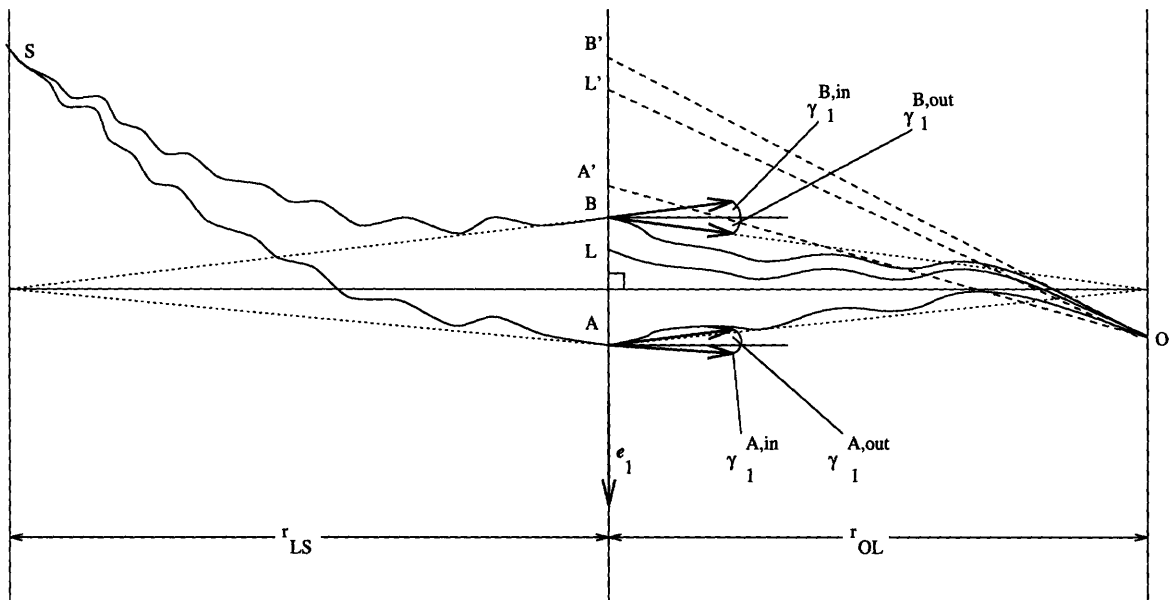
Figure 4-1: Schematic diagram of a typical lensing case, as discussed in the text. Solid lines represent true photon trajectories, dashed lines apparent trajectories as seen from the observer's position and dotted lines the unperturbed trajectories as seen from the lens plane in the absence of LSS effects. The apparent image and lens positions are denoted by A', B' and L', respectively, and can be far from the true positions.

Chapter 5

Lensing Effect on Cosmic Microwave Background Anisotropies

I present an analysis of the gravitational lensing effect on the statistical distribution of CMB anisotropies. The purpose of this work is to provide a more realistic answer concerning the importance of the lensing effect by using observational constraints on the large-scale structure distribution and properly including its evolution. For this reason I include nonlinear effects by modelling the power spectrum evolution in the nonlinear regime and I extend the calculation to nonflat universes. The method allows the calculation of the lensing effect in any standard cosmological model (i.e. in any model based on a weakly perturbed metric in a universe that is homogeneous and isotropic on large scales).

5.1   Formalism

Two photons A and B observed with an angular separation θ have a different angular separation when emitted from the last-scattering surface, $\delta\vec{\theta}^A - \delta\vec{\theta}^B$. Note that it is $\delta\vec{\theta}$ (equation B.8) that is relevant for the discussion of lensing effects on CMB, because one is interested in the angular excursion of a photon on the CMB last-

scattering surface and not in the change in its direction. Some of the previous work on this subject used the total deflection angle $\delta\vec{\gamma}$ (equation 4.2) instead of the angular excursion $\delta\vec{\theta}$. As shown in chapter 4, in $\Omega = 1$ linear theory this leads to a factor of $10^{1/2}$ overestimate of the relative dispersion between two photons. In the following I will restrict the discussion to $\delta\vec{\theta}$ and for simplicity I will drop the subscript in the dispersion, denoting it with $\sigma(\theta)$. It can be calculated from equation (B.13) by specifying the time evolution of the power spectrum $P_\phi(k, \tau)$.

Once $\sigma(\theta)$ is known as a function of θ it is straightforward to calculate the lensing effect on the CMB fluctuations. This is most easily expressed in terms of the temperature correlation function $C(\theta) = \langle (\Delta T/T)^A (\Delta T/T)^B \rangle_\theta$. Using the two-dimensional formalism (Wilson & Silk 1981; Appendix B) one obtains the modified correlation function $\tilde{C}(\theta)$,

$$\tilde{C}(\theta) = \frac{1}{\sigma^2(\theta)} \int_0^\pi \beta d\beta C(\beta) e^{-(\beta^2+\theta^2)/2\sigma^2(\theta)} I_0 \left[\frac{\theta\beta}{\sigma^2(\theta)} \right], \qquad (5.1)$$

where I_0 is the modified Bessel function of order 0. One can see that the effect of lensing is to integrate over the correlation function multiplied with approximately a gaussian centered at θ and with dispersion $\sigma(\theta)$, as can be seen using the asymptotic expansion of I_0 combined with the exponential in equation (5.1). Thus, lensing acts as a filter smoothing out the sharp features in the correlation function. For lensing to be important the correlation function at θ must be changing rapidly on a scale $\sigma(\theta)$.

One way to calculate $\sigma(\theta)$ is to use the observational constraints on the power spectrum from galaxy and velocity surveys, carefully including the effects of the power spectrum evolution in a given cosmological model, which will be explored in the next section. A somewhat less model-dependent estimate can be obtained from the observational constraints on correlated distortions of distant galaxy images. This can be described by $p(\theta)$, the average polarization within a circular aperture of radius θ, which describes the correlations in the ellipticities of galaxy images as a function of angle θ (Appendix B). Using a small argument Taylor expansion of Bessel functions in equations (B.13) and (B.15) I obtain a simple scaling between $\sigma(\theta)$ and $p(\theta)$ for an

$\Omega_{m0} = 1$ universe in the linear regime, independent of the power spectrum on small angular scales, $\sigma(\theta)/\theta = 2^{-1/2}p(\theta)(\chi_{rec}/\chi_g)^{3/2}$, where I assumed for simplicity that all the galaxies lie at a fixed distance χ_g. Nonlinear effects and $\Omega_{m0} < 1$ make the low redshift contributions more important relative to the case above, which decreases $\sigma(\theta)/\theta$ derived from $p(\theta)$. Numerical evaluation confirms this and so the scaling above can be used to give an upper limit on $\sigma(\theta)/\theta$ from the observational limits on $p(\theta)$ on arcminute scales.

5.2 Estimate of the Lensing Effect in Our Universe

In order to compute the lensing effect one needs to specify the power spectrum of potential as a function of scale and time. In the linear regime the time dependence of density perturbations in a CDM dominated universe obeys the well known growing mode solution. For the particular case of $\Omega_0 = 1$ universe the potential does not change in time and lensing contributions at early times are as important as those at late times. For the nonlinear evolution of the power spectrum I adopted the prescription by Hamilton et al. (1991), generalized to $\Omega_0 \neq 1$ by Peacock & Dodds (1994). This prescription is based on a stable clustering assumption for the evolution of the density correlation function in the nonlinear regime. Although not exact, it agrees well with the results of N-body simulations (see Peacock & Dodds 1994 and Mo, Jain & White 1995 for a detailed discussion of its applicability) and should give a good estimate of the of the power spectrum in the nonlinear regime of interest. The linear to nonlinear mapping is most easily expressed using the mass density variance $\Delta^2(k)$, which is related to the potential power spectrum via $\Delta^2(k) = 16\pi k^7 P_\phi(k)/9\Omega_m(\tau)^2 H^4 a^4$. The relation between the linear and nonlinear power spectrum is given by

$$\Delta^2(k_{nl}) = f_{nl}[\Delta^2(k_l)]; \quad k_l = [1 + \Delta^2(k_{nl})]^{-1/3}k_{nl}$$

$$f_{nl}(x) = x \left[\frac{1 + 0.2\beta x + (Ax)^{\alpha\beta}}{1 + ([Ax]^{\alpha} g^3(\Omega, a)/[11.68x^{1/2}])^{\beta}} \right]^{1/\beta}, \qquad (5.2)$$

where $A = 0.84[g(\Omega_m, \Omega_v, a)]^{0.2}$, $\alpha = 2/g(\Omega_m, \Omega_v, a)$ and $\beta = 2g(\Omega_m, \Omega_v, a)$. The linear growth factor $g(\Omega_m, \Omega_v, a)$ can be approximated with a few percent accuracy as (Lahav et al. 1991; Carroll, Press & Turner 1992)

$$g(\Omega_m, \Omega_v, a) \approx \frac{5\Omega_{m0}}{2[X(1 + [\Omega_{m0}/aX]^{0.6}) - a^2\Omega_{v0} + \Omega_{m0}/2a]}$$
$$X = 1 + \Omega_{m0}(a^{-1} - 1) + \Omega_{v0}(a^2 - 1). \qquad (5.3)$$

The system of equations presented above can be used to calculate the lensing effect on CMB for most cosmological models of current interest (the notable exception being the models with massive neutrinos on small scales where neutrino free streaming is important). Instead of presenting the results for a variety of theoretical models I will use observational constraints on the power spectrum, as compiled by Peacock & Dodds (1994), to estimate the magnitude of the effect in our universe. I will parametrize the observational power spectrum with a CDM type linear transfer function (Bardeen et al. 1986) with two free parameters, the amplitude σ_8, determined by the mass fluctuation averaged within a sphere of radius $8h^{-1}$Mpc and the shape parameter $\Omega_{m0}h$, determined by the turnover position in the power spectrum. For wavevectors between 10^{-2} and 1 hMpc^{-1} all the galaxy and cluster surveys are in a reasonable agreement with a CDM type linear power spectrum with $\Omega_{m0}h \approx 0.25$ (Peacock & Dodds 1994; da Costa et al. 1994). For normalization I will adopt $\sigma_8 = 1.0$, which is higher than the normalization obtained by Peacock & Dodds (1994) using the galaxy and cluster survey data and by White, Efstathiou & Frenk (1993) using the cluster abundances, although it is more consistent with the COBE normalization of standard CDM models (Górski et al. 1994). The adopted power spectrum is likely to be within a factor of a 2 of the real power spectrum on the dominant scales for $\sigma(\theta)$.

Using the linear power spectrum and its nonlinear evolution I computed $\sigma(\theta)/\theta$ as a function of θ for several different values of Ω_{m0} and Ω_{v0} (Figure 5-1). Thick curves give the result of a full nonlinear calculation, while the thin curves show the

corresponding linear case. One can see that while in the linear case $\sigma(\theta)/\theta$ approaches to a constant for small θ, it continues to increase in the nonlinear case. Therefore in the real universe one cannot define a typical coherence angle, which was used by previous studies (e.g. Sasaki 1989; Linder 1990a; Cayón et al. 1993a,b). The results presented here can only be used on angular scales above few arcminutes, where $\sigma(\theta)/\theta \ll 1$ and where the nonlinear mapping gives reliable estimates.

The inverse wavenumber that makes a dominant contribution to $\sigma(\theta)$ is approximately $0.5h$ Mpc^{-1} for $\theta = 1'$ and $0.05h$ Mpc^{-1} at $\theta = 1°$ and above. On angular scales larger than a few arcminutes the dominant contributions come from modes that are still in the linear regime, which can also be seen by comparing the linear and nonlinear curves on Figure (5-1). These scales are largely unaffected by the uncertainties of the nonlinear evolution and are also the scales where the large-scale observations place best constraints on the power spectrum. To test how sensitive are the results to the spectral shape I changed the spectral shape to $\Omega_{mo}h = 0.5$, keeping the σ_8 normalization unchanged. The relative difference between the two cases was a few percent only at $\theta \sim 1'$, where the dominant scales are similar to the scales that contribute to σ_8 normalization. On larger angular scales the difference between the two spectral shapes is larger (with $\Omega_{mo}h = 0.5$ having a smaller lensing effect, because it has less power on larger scales) and increases up to 50% at $\theta \sim 1°$, where the effect is however already rather small.

The lensing effect decreases with Ω_{m0}. This is mainly due to the linear decrease of potential with Ω_{m0} in the Poisson equation, partly offset by the longer travel distance, larger growth factor ratio $g(\Omega_m, \Omega_v, a)/g(\Omega_{m0}, \Omega_{v0}, a_0)$ and larger nonlinear effects in low Ω_{m0} models. The latter is more important because the scales that are nonlinear today became nonlinear earlier than the corresponding scales in an $\Omega_{m0} = 1$ universe. In the open model the universe changes from $\Omega \approx 1$ to $\Omega \ll 1$ earlier than in the cosmological constant model with the same matter density and in addition the relation between the conformal time and angular distance changes, all of which leads to a larger lensing effect. The value of $\sigma(\theta)/\theta$ linearly increases with σ_8 in the linear regime, but grows faster than that in the nonlinear regime. As discussed above the

value of σ_8 today is still somewhat uncertain. It is however unlikely that σ_8 is much bigger than 1 even in an open model and the curves on Figure (5-1) should indicate the upper range of the lensing effect in our universe. The main uncertainty in the results on arcminute scales arises currently not so much from the shape of the power spectrum, but rather from the poorly known amplitude σ_8 and the density parameter Ω_{m0}.

In Figure (5-1) I also indicated the 90 % c.l. upper limits on $\sigma(\theta)/\theta$ as derived from Mould et al. (1994) and Fahlman et al. (1994) limits on the correlated ellipticities. Both groups report a null detection of average ellipticity within a 4.8′ and 2.76′ radius aperture, respectively, with a sensitivity of about 1%. Adopting median redshifts of $z = 0.9$ and $z = 0.7$ gives radial distances 0.27 and 0.23 times the comoving distance to the horizon, respectively. For the two surveys I obtain upper limits that are comparable to the power spectrum estimates, which gives additional confidence that the effect was not severely underestimated on arcminute scales. A general conclusion that can be derived from these results is that $\sigma(\theta)/\theta$ is less than 20% on scales above 1′ and less than 5% on scales larger than 1°.

Figure (5-2) shows the lensing effect on the CMB fluctuation power spectrum for the case of $\Omega_{m0} = 1$, $\Omega_{v0} = 0$. For comparison with theoretical predictions I have computed the lensing effect on the correlation function from CMB multipole moments C_l using equation (B.21) and then Legendre transformed the correlation function using $C_l = 2\pi \int_0^\pi \sin\theta C(\theta) P_l(\cos\theta) d\theta$. The CMB power spectra C_l were obtained from a numerical integration of perturbed fluid equations in two standard adiabatic CDM models (Seljak & Bertschinger 1994). As discussed in Chapter 2 these models exhibit characteristic acoustic oscillations (Doppler peaks) and suppression on small scale due to diffusion damping. Lensing induces very little gross change in the power spectrum of CMB. However, it redistributes the power and the peaks of acoustic oscillations are smoothed because of this. On smaller angular scales they can be completely erased. This occurs both because $\sigma(\theta)/\theta$ increases and because the relative width of the oscillations becomes narrower towards smaller scales. Observational sensitivity to this effect depends on the particular experimental setup, but for most experiments

the window functions are relatively broad in l-space and consequently the effect is diluted.

5.3   Discussion

I derived the expressions to calculate the lensing effect on primary CMB anisotropies for any specified cosmological model and applied this formalism to the model which best fits the observational data on large scales. The main conclusion derived from this is that gravitational lensing does not significantly affect the CMB power spectrum on degree scales and larger, but becomes gradually more important towards smaller scales. Lensing redistributes the power in the angular correlation function and the amplitude of the effect depends on the smoothness of the underlying CMB spectrum. For standard adiabatic CDM models the Doppler peaks are rather prominent even at small angular scales (beyond $l \approx 1000$) and lensing may completely smooth this structure.

Recently, two groups claimed that the gravitational lensing effect on CMB has been severely underestimated in previous calculations and that it importantly changes the CMB pattern even on degree angular scales. Bassett et al. (1994) assume a model in which photons propagate through a homogeneous universe with a density smaller than its mean density to account for the fact that some of the mass resides in dense clumps. Using the Dyer-Roeder distance-redshift relation in such a universe they obtain an increase in angular separation between the two photons relative to its unperturbed value. Similarly, Fukushige et al. (1994) assume a model in which the universe is populated by a number of massive clumps embedded in a large empty void. Here the angular separation between two photons is additionally increased with every passage of the photons by a clump, because the closer photon is always deflected more than the more distant one. This leads to an exponential growth of the angular separation until it reaches the mean projected separation between the clumps. One problem with these models is that they cannot be applied to large (supercluster) scales, where the density fluctuations are small, given that in these models the mass

74

density in a box on scales smaller than the mean distance between the clumps is either zero or very large. Observational data on large scales suggest that density fluctuations are close to gaussian and both underdensities and overdensities have to be included for a proper description of large-scale structure. The effect of underdensities is to decrease the angular separation between the two photons and this leads to a random walk growth of rms deviation between them. Numerical studies of light propagation in realistic models (Jaroszynski et al. 1991) confirm that there are no large distortions in the relative photon trajectories present for most lines of sight, at least on scales above the resolution scale of few arcseconds. Moreover, flux conservation requires that exponential growth in separation between photons passing on the same side of a clump is balanced by a strong focusing between photons that pass on the opposite sides of the clump. This would lead to multiple images (strong lensing), but it is known observationally that such situations are rare in our universe. It is nevertheless possible that in a highly nonlinear regime a universe could be approximated by the models discussed by Fukushige et al. (1994) and Bassett et al. (1994). In such a regime our model would predict relative fluctuations larger than unity and its predictions would become unreliable, because the assumption that the potential deflecting the photons can be calculated along the unperturbed paths would not be satisfied. As long as $\sigma(\theta)/\theta$ remains small this is not the case and for the density fluctuations as measured in our universe this condition is satisfied at least on angular scales above a few arcseconds.

Although gravitational lensing is of small significance for the present day CMB experiments, mostly sensitive to degree angular scales, it may become relevant for the future experiments that will probe smaller angular scales with a much higher sensitivity and sky coverage. Gravitational lensing effect will be especially important for the high precision determination of cosmological parameters planned for the next generation of experiments and the uncertainties caused by the gravitational lensing should be included in the modelling of extraction of cosmological parameters from the CMB measurements. The formalism developed in this paper allows to calculate the lensing effect on CMB for any specified cosmological model and can be included

as a postprocessor to the standard calculations of CMB multipole moments.

.

Bibliography

[1] Bardeen, J. M., Bond, J. R., Kaiser, N., & Szalay, A. S. 1986, ApJ, 304, 15

[2] Bassett, B. A. C. C., Dunsby, P. K. S. & Ellis, G. F. R. 1994, to be published, Phys. Rev. D

[3] Blandford, R. D., & Jaroszynski, M. 1981, ApJ, 246, 1

[4] Blanchard, A. and Schneider, J., 1987, A&A, 184, 1

[5] Carroll, S. M., Press, W. H., & Turner, E. L. 1992, ARA&A, 30, 499

[6] Cayón, L., Martínez-González, E., & Sanz, J. L. 1993a, ApJ, 403, 471

[7] Cole, S. and Efstathiou, G., 1989, MNRAS, 239, 195

[8] da Costa, L. N., Vogeley, M. S., Geller, M. J., Huchra, J. P., & Park, C. 1994, ApJ, 437, L1

[9] Fahlman, G. G., Kaiser, N., Squires, G. & Woods, D. 1994, ApJ, 437, 56

[10] Fukushige, T., Makino, J., & Ebisuzaki, T. 1994, ApJ436, L107

[11] Górski K. M. et al. 1994, ApJ, 430, L89

[12] Hamilton, A. J. S., Kumar, P., Lu, E., & Matthews, A. 1991, ApJ, 374, L1

[13] Jaroszynski, M., Park, C., Paczynski, B., & Gott, J., R., III 1991, ApJ, 365, 22

[14] Lahav, O., Lilje, P. B., Primack, J. R., Rees, M. J. 1991, MNRAS, 251, 128

[15] Linder, V. E. 1990, MNRAS, 243, 353

[16] Mo, H. J., Jain, B. & White, S. D. M., submitted to MNRAS

[17] Mould, J., Blandford, R., Villumsen, J., Brainerd, T., Smail, I., Small, T., & Kells, W. 1994, Caltech preprint

[18] Peacock, J. A., & Dodds, S. J. 1994, MNRAS, 267, 1020

[19] Sasaki, M. 1989, MNRAS, 240, 415

[20] Seljak U., 1994, ApJ, 436, 509

[21] Seljak, U., & Bertschinger, E. 1994, in "Present and Future of the Cosmic Microwave Background", eds. J. L. Sanz, E. Martinez-Gonzalez, & L. Cayón (Springer-Verlag: Berlin), p. 165

[22] White, S. D. M., Efstathiou, G., & Frenk C. S. 1993, MNRAS, 262, 1023

[23] Wilson, M. L., & Silk, J. 1981, ApJ, 243, 14
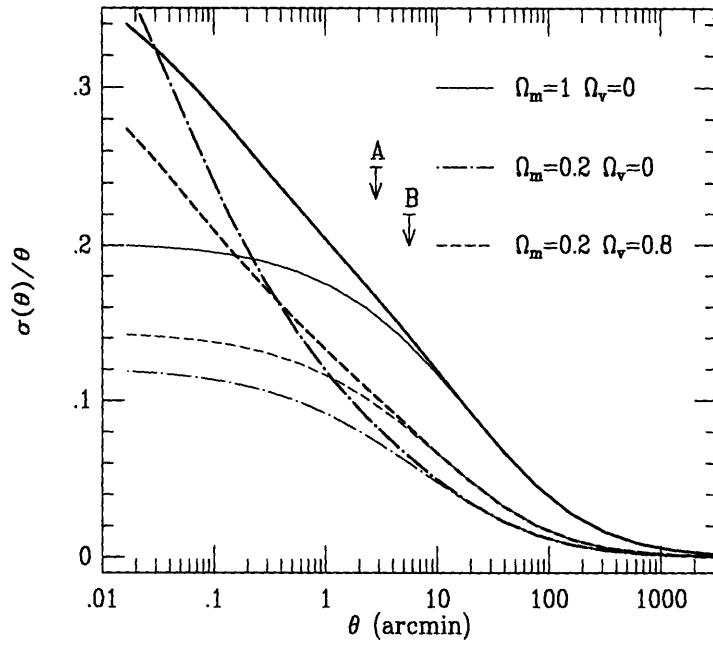
Figure 5-1: $\sigma(\theta)/\theta$ versus θ for 3 different values of Ω_{m0} and Ω_{v0}. Thick lines are the result of a full nonlinear calculation, while the thin lines give the corresponding linear case. Also indicated are the 90% c.l. upper limits from ellipticity correlations of distant galaxies, as derived from observations by Fahlman et al. (1994) (A) and Mould et al. (1994) (B).
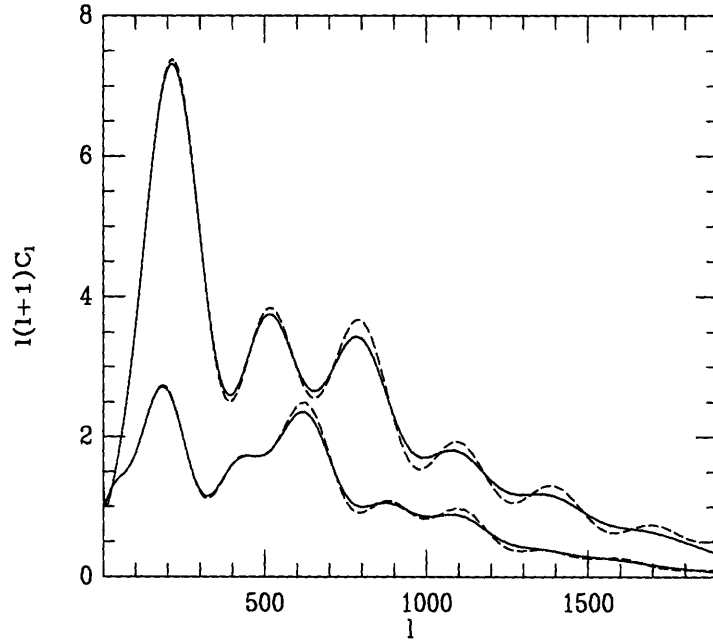
Figure 5-2: Quadrupole normalized CMB anisotropy power spectrum $l(l+1)C_l$ versus l with lensing (solid lines) and without lensing (dashed lines). Upper curves are for adiabatic CDM model with $\Omega_{b0} = 0.03$, $h = 0.8$, $\Omega_{m0} = 0.2$ and $\Omega_{v0} = 0.8$, lower curves are for adiabatic CDM model with $\Omega_{b0} = 0.05$, $h = 1$, $\Omega_{m0} = 1$ and $\Omega_{v0} = 0$. Lensing smoothes the sharp features in the power spectrum, but leaves the overall shape unchanged.

Appendix A

Relativistic Perturbation Theory

In this Appendix I present the equations needed for calculations of the photon energy distribution in a weakly perturbed Robertson-Walker spacetime. The choice of coordinate system corresponds to the generalization of the so-called longitudinal gauge. The main advantage of this gauge compared to other gauge choices is that perturbation theory remains valid even when density perturbations become large and gives the cosmological generalization of Newtonian gravity. Metric perturbations in this gauge correspond exactly to several of the gauge-invariant variables introduced by Bardeen (1980), but by imposing the explicit gauge conditions the mathematical analysis is simplified. Most of the material presented here has been derived elsewhere (Wilson 1981; Kodama & Sasaki 1984; Abbott & Schaefer 1986; Bond & Efstathiou 1987; Ma & Bertschinger 1995; Bertschinger 1995), so I will restrict the presentation to the final results only.

A.1   Metric, Geodesic and Field Equations

The framework is a perturbed flat Robertson-Walker with small-amplitude metric fluctuations. In the most general form one can write the line element using conformal time τ and comoving coordinates x^i as

$$ds^2 = a^2(\tau) \left\{ -(1 + 2\psi)d\tau^2 + 2w_i d\tau dx^i + [(1 - 2\phi)\gamma_{ij} + 2h_{ij}] dx^i dx^j \right\}. \quad (A.1)$$

Here $a(\tau)$ is the scale factor expressed in terms of conformal time. I will adopt units such that $c = 1$. The space part of the background metric can be written as

$$\gamma_{ij}dx^i dx^j = d\chi^2 + r^2(d\theta^2 + \sin^2\theta d\phi^2),$$

$$r = \sin_K \chi \equiv \begin{cases} K^{-1/2}\sin K^{1/2}\chi, & K > 0 \\ \chi, & K = 0 \\ (-K)^{-1/2}\sinh(-K)^{1/2}\chi, & K < 0 \end{cases} \qquad (A.2)$$

where K is the curvature term which can be expressed using the present density parameter Ω_0 and the present Hubble parameter H_0 as $K = (\Omega_0 - 1)H_0^2$. The density paramater Ω_0 can have contributions from mass density Ω_{m0} or vacuum energy density Ω_{v0}, $\Omega_0 = \Omega_{m0} + \Omega_{v0}$. The subscript 0 denotes the values at present time. The advantage of using the conformal time τ is that the metric becomes conformally Euclidean ($K = 0$), 3-sphere ($K > 0$) or 3-hyperboloid ($K < 0$) and leads to a simple geometrical description of light propagation.

In equation (A.1) I introduced two scalar fields $\psi(\vec{x}, \tau)$ and $\phi(\vec{x}, \tau)$, one 3-vector field $\vec{w}(\vec{x}, \tau)$ and one symmetric traceless second-rank tensor $\overleftrightarrow{h}(\vec{x}, \tau)$. I will assume that the metric perturbations are small and neglect all the higher order terms. The gauge freedom allows to impose the following gauge conditions on metric components (Bertschinger 1995),

$$\vec{\nabla} \cdot \vec{w} = 0 , \quad \vec{\nabla} \cdot \overleftrightarrow{h} = 0 . \qquad (A.3)$$

In the absence of scattering, emission or absorption the photon propagation is governed by the geodesic equation,

$$\frac{dp^\mu}{d\lambda} + \Gamma^\mu_{\nu\tau}p^\nu p^\tau = 0 , \ p^\mu = \frac{dx^\mu}{d\lambda} \qquad (A.4)$$

Here λ is the affine parameter and $\Gamma^\mu_{\nu\tau}$ are the affine connection coefficients. The geodesic equation can be decomposed into time and space components. The time

part governs the photon energy evolution. Applied to the metric above it gives

$$\frac{d\ln(aE)}{dl} = -\vec{n} \cdot \vec{\nabla}\psi + \dot{\phi} - \vec{n} \cdot \dot{\vec{w}} - \vec{n} \cdot \dot{\overset{\leftrightarrow}{h}} \cdot \vec{n}, \qquad (A.5)$$

where $\vec{n}$ is the photon direction, E its energy and the affine parameter dl is the comoving path length along the geodesic. For photons propagating in the radial or nearly radial direction one has $dl \approx d\tau \approx -d\chi$. The relation between the radial distance χ and conformal time τ is in the lowest order given by $\chi = \tau_0 - \tau$.

Einstein's equation $G^\nu_\mu = 8\pi G T^\nu_\mu$ applied to the background metric gives the evolution of the expansion factor $a(\tau)$,

$$\left(\frac{\dot{a}}{a}\right)^2 \equiv \eta^2 = \frac{8\pi}{3} G \bar{\rho} a^2 - K, \quad \dot{\eta} = -\frac{4\pi}{3} G a^2 (\bar{\rho} + 3\bar{p}). \qquad (A.6)$$

Overdots denote derivatives with respect to the conformal time τ. The mean density of the universe $\bar{\rho}$ (and similarly the mean pressure $\bar{p}$) can be written as a sum of matter, radiation and vacuum contributions,

$$\bar{\rho} = \bar{\rho}_{m0} a^{-3} + \bar{\rho}_{r0} a^{-4} + \bar{\rho}_{v0} \qquad (A.7)$$

The perturbed stress-energy tensor T^μ_ν can be written in terms of physical quantities:

$$T^0_0 = -\rho, \ T^i_0 = -(\rho + p)v^i, T^0_i = (\rho + p)(v_i + w_i), \ T^i_j = p\delta^i_j + \Sigma^i_j, \qquad (A.8)$$

where v^i is the coordinate 3-velocity and anisotropic stress Σ^i_j is a traceless tensor that can be further decomposed into parallel (scalar), perpendicular (vector) and transverse-traceless (tensor) parts:

$$\overset{\leftrightarrow}{\Sigma} = \overset{\leftrightarrow}{\Sigma}_\| + \overset{\leftrightarrow}{\Sigma}_\perp + \overset{\leftrightarrow}{\Sigma}_T, \vec{\nabla} \times (\vec{\nabla} \cdot \overset{\leftrightarrow}{\Sigma}_\|) = \vec{\nabla} \cdot (\vec{\nabla} \cdot \overset{\leftrightarrow}{\Sigma}_\perp) = \vec{\nabla} \cdot \overset{\leftrightarrow}{\Sigma}_T = 0. \qquad (A.9)$$

Similarly one can decompose the momentum density into parallel and perpendicular

parts:

$$(\rho + p)\vec{v} = (\rho + p)\vec{v}_\parallel + (\rho + p)\vec{v}_\perp, \vec{\nabla} \times (\rho + p)\vec{v}_\parallel = \vec{\nabla} \cdot (\rho + p)\vec{v}_\perp = 0. \quad \text{(A.10)}$$

The perturbed Einstein's equations separate according to the spatial geometry into scalar, vector and tensor parts (Bertschinger 1995),

$$(\nabla^2 + 3K)\phi - 3\eta \left(\dot{\phi} + \eta\psi\right) = 4\pi Ga^2(\rho - \bar{\rho}) \ ,$$

$$\vec{\nabla}(\dot{\phi} + \eta\psi) = 4\pi Ga^2 \left[(\rho + p)(\vec{v} + \vec{w})\right]_\parallel \ ,$$

$$(\nabla^2 + 2K)\vec{w} = 16\pi Ga^2 \left[(\rho + p)(\vec{v} + \vec{w})\right]_\perp \ ,$$

$$\ddot{\phi} - K\phi + \eta(\dot{\psi} + 2\dot{\phi}) + (2\dot{\eta} + \eta^2)\psi + \frac{1}{3}\nabla^2(\phi - \psi) = 4\pi Ga^2(p - \bar{p}) \ ,$$

$$\left(\nabla_i\nabla_j - \frac{1}{3}\delta_{ij}\nabla^2\right)(\psi - \phi) = 8\pi Ga^2 \Sigma_{ij,\parallel} \ ,$$

$$-\left(\partial_\tau + 2\eta\right)\nabla_{(i}w_{j)} = 8\pi Ga^2 \Sigma_{ij,\perp} \ ,$$

$$\left(\partial_\tau^2 + 2\eta\partial_\tau - \nabla^2 + 2K\right)h_{ij} = 8\pi Ga^2 \Sigma_{ij,\mathrm{T}} \ , \quad \text{(A.11)}$$

where I have denoted symmetrization with parentheses $\nabla_{(i}w_{j)} = (\nabla_i w_j + \nabla_j w_i)/2$ and raising and lowering of spatial indices is performed with the background metric γ_{ij}. The energy-momentum tensor is required to obey local conservation law $T^{\mu\nu}_{;\mu} = 0$, which in the weak-field limit becomes

$$\dot{\rho} + 3(\rho + p)(\eta - \dot{\phi}) + \vec{\nabla} \cdot (\rho + p)\vec{v} = 0,$$

$$\left(\frac{\partial}{\partial_\tau} + 4\eta\right)(\rho + p)(\vec{v} - \vec{w}) + \vec{\nabla}p + \vec{\nabla} \cdot \overleftrightarrow{\Sigma} + (\rho + p)\vec{\nabla}\psi = 0. \quad \text{(A.12)}$$

A.2 Boltzmann and Fluid Equations for Scalar Perturbations

In this section I present the system of evolution equations for matter and radiation. For compactness I will restrict the application in the following to the scalar fluc-

tuations, given that they make the dominant contribution to the cosmic microwave background anisotropies and gravitational lensing.

Matter content of the universe can be divided into two classes. In the first class there are matter components which can be well described with the fluid approximation. This class includes cold dark matter and baryons. To specify their evolution one only needs the equations for overdensity $\delta = \rho/\bar{\rho} - 1$ and velocity $\vec{v}$, both of which can be obtained from energy-momentum conservation equation (A.12). Expanding the sources in terms of scalar harmonics Q defined as the eigenfunction solution of

$$\nabla^2 Q + k^2 Q = 0 \qquad (A.13)$$

one obtains the following set of equations,

Cold dark matter —

$$\dot{\delta_c} = -kv_c + 3\dot{\phi}, \quad \dot{v_c} = -\frac{\dot{a}}{a}v_c + k\psi. \qquad (A.14)$$

Because photons scatter off free electrons (Thomson scattering) one must explicitly include the exchange of momentum between the photons and baryons in the momentum conservation equation. This leads to the following equations,

Baryons—

$$\begin{aligned}
\dot{\delta_b} &= -kv_b + 3\dot{\phi}, \\
\dot{v_b} &= -\frac{\dot{a}}{a}v_b + \frac{4\bar{\rho}_\gamma}{3\bar{\rho}_b}an_e x_e \sigma_T(v_\gamma - v_b) + k\psi.
\end{aligned} \qquad (A.15)$$

where n_e is the electron density, x_e the ionization fraction and σ_T Thomson cross section.

In the second class are matter components for which the full phase space distribution function $f(\vec{x}, \vec{p}, \tau)$ is required. This class includes neutrinos (both massless and massive) and photons. Here I will restrict the discussion to the massless neutrinos

and photons. Their evolution is governed by the Boltzmann equation

$$\frac{df(\vec{x},\vec{p},\tau)}{d\tau} = \frac{\partial f}{\partial \tau} + \frac{\partial f}{\partial x^i}\frac{dx^i}{d\tau} + \frac{\partial f}{\partial p}\frac{dp}{d\tau} + \frac{\partial f}{\partial n^i}\frac{dn^i}{d\tau} = \left(\frac{df(\vec{x},\vec{p},\tau)}{d\tau}\right)_c, \qquad (A.16)$$

where $\vec{p} = p\vec{n}$ is the momentum of the particles and the term on the right hand side is the collision term (absent in the case of collisionless neutrinos). The distribution function f can be expanded to the first order,

$$f(\vec{x},\vec{p},\tau) = f_0(p) + f_1(\vec{x},\vec{p},\tau). \qquad (A.17)$$

The zero-order phase space distribution is the Planck distribution for photons or Fermi-Dirac distribution for neutrinos $f_0(p) \propto (4\pi^3(e^{\hbar p/kT} \pm 1))^{-1}$.

It is useful to integrate the perturbed distribution function over the momentum and expand it in a generalized Legendre series,

$$\Delta(\vec{n},\tau) = \frac{\int dp\, p^3 f_1}{4\int dp\, p^3 f_0} = \sum_{l=0}^{\infty}(2l+1)\Delta_l(-k)^{-l}Q_{;i...j}P_l^{i...j}, \qquad (A.18)$$

where $\vec{n}$ is the direction of the photon and $P_l^{i...j}$ is defined recursively as

$$P_0 = 1, \; P_1^i = n^i, \; P_{l+1}^{ijk...m} = \frac{2l+1}{l+1}n^{(i}P_l^{jk...m)} - \frac{l}{l+1}\gamma^{(ij}P_{l-1}^{k...m)}. \qquad (A.19)$$

In the flat space this reduces to the usual Legendre expansion $\Delta = \sum_l(2l+1)\Delta_l P_l(\vec{k}\cdot\vec{n})$, where P_l are the Legendre polynomials of order l. After momentum integration the Boltzmann equation for massless neutrinos becomes,

$$\dot{\Delta}_\nu + \vec{n}\cdot\vec{\nabla}\Delta_\nu = \dot{\phi} - \vec{n}\cdot\vec{\nabla}\psi. \qquad (A.20)$$

From this one obtains the following hierarchy of coupled evolution equations,

Massless neutrinos—

$$\dot{\delta}_\nu \equiv 4\dot{\Delta}_{\nu,0} = -\frac{4}{3}kv_\nu + 4\dot{\phi},$$

85

$$\dot{v}_\nu \equiv 3\Delta_{\nu,1} = k\left[\Delta_{\nu,0} - 2\left(1 - \frac{3K}{k^2}\right)\Delta_{\nu,2} + \psi\right]$$

$$\dot{\Delta}_{\nu,2} = \frac{k}{5}\left[\frac{2}{3}v_\nu - \frac{3}{5}\left(1 - \frac{8K}{k^2}\right)\Delta_{\nu,3}\right],$$

$$\dot{\Delta}_{\nu,l} = \frac{k}{2l+1}\left[l\Delta_{\nu,l-1} - (l+1)\left(1 - \frac{l(l+1)K}{k^2}\right)\Delta_{\nu,l+1}\right]. \quad (A.21)$$

Photons interact with electrons and one needs to add the collision term in equation (A.16). In terms of temperature anisotropies and keeping only the the lowest order terms it is given by (Kodama & Sasaki 1986)

$$\dot{\Delta}_\gamma + \vec{n}\cdot\vec{\nabla}\Delta_\gamma = \dot{\phi} - \vec{n}\cdot\vec{\nabla}\psi + \dot{\Delta}_c$$

$$\dot{\Delta}_c = an_e x_e \sigma_T(\Delta_{\gamma 0} + \vec{n}\cdot\vec{v}_b + \frac{3}{16}\vec{n}\cdot\overleftrightarrow{\Pi}_\gamma\cdot\vec{n}), \quad (A.22)$$

where $\overleftrightarrow{\Pi}_\gamma$ is related to the photon anisotropic stress, $\overleftrightarrow{\Sigma}_\gamma = 8\pi G\bar{\rho}_\gamma\overleftrightarrow{\Pi}_\gamma$. In equation (A.22) I neglected photon polarization. The hierarchy becomes

Photons—

$$\dot{\delta}_\gamma \equiv 4\Delta_{\gamma,0} = -\frac{4}{3}kv_\gamma + 4\dot{\phi},$$

$$\dot{v}_\gamma \equiv 3\Delta_{\gamma,1} = k\left[\Delta_{\gamma,0} - 2\Delta_{\gamma,2}\left(1 - \frac{3K}{k^2}\right) + \psi\right] + an_e\sigma_T(v_b - v_\gamma),$$

$$\dot{\Delta}_{\gamma 2} = \frac{k}{5}\left[\frac{2}{3}v_\gamma - 3\left(1 - \frac{8K}{k^2}\right)\Delta_{\gamma,3}\right] - \frac{9}{10}an_e\sigma_T\Delta_{\gamma,2}, \quad (A.23)$$

$$\dot{\Delta}_{\gamma,l} = \frac{k}{2l+1}\left[l\Delta_{\gamma,l-1} - (l+1)\left(1 - \frac{l(l+1)K}{k^2}\right)\Delta_{\gamma,l+1}\right] - an_e\sigma_T\Delta_{\gamma,l}.$$

A.3 Integral Solution for Temperature Anisotropies

Instead of solving the equations presented in previous section in general one may solve them only for the photons that reach the observer at $\chi = 0$. These photons move along radial geodesics and their direction vector $\vec{n}$ is just opposite to the observed direction. Integrating the photon Boltzmann equation (A.22) along the radial geodesics one

obtains the following integral solution for $\Delta_\gamma + \psi$,

$$[\Delta_\gamma(\vec{n}) + \psi](\chi = 0) = \int_0^{\chi_0 = \tau_0} \left[\dot{\mu} \left(\psi + \frac{\delta_\gamma}{4} + \vec{n} \cdot \vec{v}_b + \frac{3}{16} \vec{n} \cdot \overset{\leftrightarrow}{\Pi}_\gamma \cdot \vec{n} \right) + \dot{\phi} + \dot{\psi} \right] e^{-\mu} d\chi.$$

(A.24)

I introduced the Thomson opacity along the past light cone $\mu(\chi) = \int_0^\chi \dot{\mu}(\chi') d\chi'$ with $\dot{\mu} = a x_e n_e \sigma_T$. Apart from the unobservable monopole contribution arising from the local gravitational potential equation (A.24) gives the temperature anisotropy in the direction of the photon $\vec{n}$ today.

Both $\vec{v}_b$ and $\overset{\leftrightarrow}{\Pi}_\gamma$ can be expressed in terms of scalar quantities, $\vec{v}_b = \vec{\nabla} \psi_b$ and $\Pi_\gamma^{ij} = (\nabla^i \nabla^j - \gamma^{ij} \nabla^2 / 3) \psi_\Pi$. The corresponding terms in equation (A.24) can be rewritten in terms of radial partial derivatives as $-\partial_\chi \psi_b$ and $(\partial_\chi \partial_\chi - \nabla^2 / 3) \Psi_\Pi$.

The temperature anisotropy in the sky $\Delta_\gamma(\vec{n})$ can be expanded in spherical harmonic basis as

$$\Delta_\gamma(\vec{n}) = \sum_{lm} a_{lm} Y_{lm}(\vec{n}).$$

(A.25)

The spherical expansion coeficients can be calculated from

$$a_{lm} = \int d\Omega Y_{lm}^*(\vec{n}) \Delta_\gamma(\vec{n}).$$

(A.26)

The mean square of this quantity gives the multipole moments of cosmic microwave fluctuations, $|a_l|^2 \equiv C_l = \langle |a_{lm}|^2 \rangle$, where the brackets denote ensemble average. The angular correlation function is related to the power spectrum

$$C(\theta) = \langle \Delta(\vec{n}_1) \Delta(\vec{n}_2) \rangle_{\vec{n}_1 \cdot \vec{n}_2 = \cos\theta} = \frac{1}{4\pi} \sum_{l=0}^\infty (2l+1) C_l P_l(\cos\theta).$$

(A.27)

It is convenient to expand the sources in equation (A.24) in a spherical basis (Abbott & Schaefer 1986)

$$Q(\vec{x}) = 4\pi k \Phi_\beta^l(\chi) Y_{lm}(\vec{n}),$$

(A.28)

where $\beta^2 = k^2 + K$. The radial functions $\Phi_\beta^l(\chi)$ are the so-called ultra-spherical Bessel functions. In flat space limit they reduce to the usual spherical Bessel functions $j_l(k\chi)$.

I will not present their explicit expressions here, but refer the reader to Abbott &
Schaefer (1986), who give the general formulae for calculating $\Phi_\beta^l(\chi)$.

Using equations (A.24)-(A.26) and orthonormality of spherical harmonics one ob-
tains the following expression for the multipole moments[1],

$$
C_l = (4\pi)^2 \int \beta^2 P(\beta) d\beta D_l^2(\beta)
$$

$$
D_l(\beta) = \int_0^{\chi_0} \left[\dot{\mu} \left(\psi + \frac{\delta_\gamma}{4} \right) \Phi_\beta^l(\chi) + v_b \Phi_\beta^{ll}(\chi) + (\dot{\phi} + \dot{\psi}) \Phi_\beta^l(\chi) \right] e^{-\mu} d\chi, \quad (A.29)
$$

where χ and τ are related through $\chi = \tau_0 - \tau$. I neglected the photon anisotropic
stress and polarization contributions, both of which lead to a negligible error on
large scales and up to a 10% error on scales around $l \approx 1000$ (Bode & Bertschinger
1995). $P(\beta)$ is the primordial power spectrum of potential, often expressed as a power
law $P(\beta) \propto \beta^{n-4}$, while $\Phi_\beta^{ll}(\chi)$ denotes the derivative of the ultra-spherical Bessel
function with respect to $\beta\chi$ and can be expressed in terms of the ultra-spherical
Bessel functions as (Abbott & Schaefer 1986)

$$
\Phi_\beta^{ll}(\chi) = \cos_K \chi \frac{l}{\beta \sin_K \chi} \Phi_\beta^l(\chi) - \left[1 - \frac{K(l+1)^2}{\beta^2} \right] \Phi_\beta^{l+1}(\chi), \quad (A.30)
$$

where I defined

$$
\cos_K \chi \equiv \begin{cases} \cos K^{1/2}\chi, & K > 0 \\ 1, & K = 0 \\ \cosh(-K)^{1/2}\chi, & K < 0. \end{cases} \quad (A.31)
$$

The source terms δ_γ, v_b, ψ and ϕ are functions of the wavenumber k and time τ and
can be calculated from equations presented in the previous section. Equation (A.29)
is an integral equation, since it couples the first two photon multipoles on the left and
right hand side. Although it is not adequate for solving the time evolution of photon
density and velocity, it is nevertheless useful if one wants to understand different

---

[1]In a closed universe the integration over β is replaced with summation over integer values of
$K^{1/2}\beta$.

physical effects that contribute to C_l's. It is also a starting point for approximate methods, which are explored in Chapter 2.

For completeness I give below the corresponding solutions for vector and tensor modes, again neglecting photon anisotropic stress and polarization. Only the radial eigenfunctions are needed and are given by (Abbott & Schaefer 1986)

$$\Phi_r^{(v)} = \sqrt{l(l+1)}\frac{\Phi_\beta^l(\chi)}{\beta \sin_K \chi}\,,\ \beta^2 = k^2 + 2K,$$

$$\Phi_{rr}^{(t)} = \sqrt{\frac{(l+2)!}{2\beta^2(\beta^2 - K)(l-2)!}\frac{\Phi_\beta^l(\chi)}{\sin_K^2 \chi}}\,,\ \beta^2 = k^2 + 3K. \qquad (A.32)$$

The C_l's can be calculated from the same expression as in equation (A.29) using the D_l's given by

$$D_l^{(v)} = \sqrt{l(l+1)}\int_0^{\chi_0} \frac{1}{\beta \sin_K \chi}\, [\mu v_b - \dot{w}]\,\Phi_\beta^l(\chi)e^{-\mu}d\chi$$

$$D_l^{(t)} = \sqrt{\frac{(l+2)!}{2\beta^2(\beta^2 - K)(l-2)!}}\int_0^{\chi_0} \frac{-\dot{h}\Phi_\beta^l(\chi)}{\sin_K^2 \chi}e^{-\mu}d\chi. \qquad (A.33)$$

A.4 Limber's Equation

The general solution in equation (A.29) simplifies considerably if one is considering small angular scales and if the fluctuations at widely separated points can be considered statistically independent (a fair sample criterion). The latter condition is satisfied if the window function $\dot{\mu}\exp(-\mu)$ or $\dot{\phi}\exp(-\mu)$ is broad compared to the largest correlation length, as it is the case if there was an epoch of late reionization or a late epoch of time dependent gravitational potential. In the latter case the condition above is satisfied because correlations at a distance k^{-1} are slowly changing on a time scale ck^{-1}, since weak field gravity can only produce nonrelativistic motions. The radial integral in equation (A.29) is thus a product of spherical Bessel function $j_l(kr)$ (restricting for simplicity to the flat universe; the term with $j_l(kr)'$ can be rewritten into a total derivative plus a partial derivative with respect to time τ) and a slowly changing function of time. For large l the spherical Bessel function $j_l(x)$ is

exponentially suppressed for $x \ll l$ and is rapidly oscillating for $x \gg l$. The integral in equation (A.29) is thus 0 for $kr \ll l$, jumps to a certain value determined by the slowly varying function at $kr = l$ and oscillates about it for $kr \gg l$. The integral may be approximated by removing the slowly changing part and using the large l approximation,

$$\int_0^x j_l(x')dx' = \begin{cases} 0, & x < l \\ \sqrt{\frac{\pi}{2l}}, & x \geq l \end{cases} \tag{A.34}$$

One can apply this approximation to the case where $\dot{\phi}$ is changing with time in the late epoch of evolution, which leads to the line-of-sight integral contribution to temperature anisotropies (the so-called integrated Sachs-Wolfe effect). The contributions are coming from a broad region in space, so that the fair sample criterion is satisfied on small angular scales, where the dominant wavelengths are much shorter than the typical size of the potential visibility function $\dot{\phi}\exp(-\mu)$. Combining equations (A.29) and (A.34) one obtains the Fourier space analogue of Limber's equation (Limber 1954; Peebles 1980; Kaiser 1992),

$$\begin{aligned} C_l^{(isw)} &= 4(4\pi)^2 \int_0^\infty P_{\dot{\phi}}[k, \tau = \tau_0 - l/k]\frac{\pi}{2l}S(kr_{\rm rec} - l)dk \\ &= 32\pi^3 \int_0^{\chi_0} P_{\dot{\phi}}(l/r, \tau = \tau_0 - \chi)\frac{d\chi}{r^2}, \end{aligned} \tag{A.35}$$

where $r_{\rm rec}$ is the angular distance to the last-scattering surface, $S(x)$ is a step function being 0 below x and 1 above it and $P_{\dot{\phi}}(k,\tau)$ is the power spectrum of $\dot{\phi}$ at time τ. Although the derivation above is only valid in a flat universe, the final expression can be used also in a non-flat universe, provided that r is interpreted as the angular distance, $r = \sin_K \chi$. Most of the contribution to the integral comes from rather low redshifts ($z < 10$) where Thomson damping term $\exp(-\mu)$ is negligible even in a reionized universe, which justifies its omission in equation (A.35). I assumed that the power spectrum is not changing over ck^{-1}, but restored its slow time dependence in the radial integral in equation (A.35). Since only the two-point statistics are studied one can use the above equation both in the linear and in the nonlinear regime (where the distribution of $\dot{\phi}$ is nongaussian). In the nonlinear regime the potential is

changing with time and anisotropies are created in any cosmological model. This is the Rees-Sciama effect and is explored in detail in Chapter 3.

Limber's equation can also be applied to other late-time sources of anisotropies. Although these are not studied in this thesis I will present for completeness their general expressions below (for a more detailed study of some of these processes, see Persi et al. 1995). A first example is the primary anisotropy in a reionized universe. In equation (A.24) the velocity part of Thomson scattering is proportional to

$$n_e x_e \vec{n} \cdot \vec{v} = \bar{n}_e x_e (1 + \delta_b) \vec{n} \cdot \vec{v} \equiv \bar{n}_e x_e \vec{n} \cdot \vec{p}. \qquad (A.36)$$

After recombination when Compton drag on baryons becomes negligible baryons follow dark matter and one may approximate δ_b with δ_c (this approximation breaks down again in the very nonlinear stages of evolution). In this case $\vec{p}$ is proportional to the matter momentum density. It can be decomposed into a parallel and perpendicular component (as in equation A.10). The parallel component suffers significant cancellation, because if the integrand in equation (A.24) can be written as a total derivative then peak and trough contributions to ΔT cancel out exactly. In reality some contribution remains, because the integrand cannot be written as a total derivative as both the velocity potential ψ_v and the visibility function $\dot{\mu} \exp(-\mu)$ are time dependent. Using similar methods as above and including the contribution from δ_γ I obtain for the primary (linear) contribution,

$$C_l^{\text{reion}} = 8\pi^3 \int_0^{\chi_0} \frac{d\chi}{r^2} \left(\ddot{\mu} - \dot{\mu}^2 + \dot{\mu} \frac{d \ln}{d\tau} [HfaD_+] \right)^2 e^{-2\mu} k^{-4} (HfaD_+)^2 P_\delta(k = l/r), \qquad (A.37)$$

where $f(\Omega) \approx \Omega^{0.6}$, H is the Hubble constant and $P_\delta(k)$ is the density power spectrum today.

Another source of anisotropies is arising from the perpendicular component or the vector part of $\vec{p}$, which does not suffer the same cancellation as above. Because of this its contribution is actually much larger than the contribution from equation (A.37), despite the fact that it vanishes in the linear regime. This is the so-called

Vishniac term (Vishniac 1987). It can be computed using the radial vector harmonic expansion as in equation (A.33). Following the same approximations as in the scalar case I obtain

$$C_l^{(V)} = 8\pi^3 \int_0^{\chi_0} \frac{d\chi}{r^2} \left(\dot{\mu} e^{-\mu} \right)^2 P_{p\perp}(k = l/r, \tau = \tau_0 - \chi),$$

(A.38)

where $P_{p\perp}(k)$ is the perpendicular momentum density power spectrum. Comparison between equations (A.37) and (A.38) shows that the primary contribution is suppressed relative to the secondary approximately by $(k\eta)^{-2}$.

In clusters where plasma is ionized and heated to a high temperature the CMB photons are also scattering off the thermal electrons. This is the so-called Sunyaev-Zel'dovich (1980) effect (henceforth SZ). In this case the role of momentum density is taken by the pressure of the gas,

$$\Delta T_{RJ}(\vec{n}) = -2 \int_0^{\chi_0} \frac{a\sigma_T}{m_e} p d\chi$$

(A.39)

where p is the electron pressure and m_e the electron mass. Again I neglected the damping term $\exp(-\mu)$, given that the SZ contribution is dominant at low redshifts. In contrast to other anisotropies discussed in this thesis SZ distortions are frequency dependent, which provides an additional discriminator to separate them from the primary anisotropies. The subscript RJ indicates that the expression is only valid in the Rayleigh-Jeans portion of the spectrum. The SZ contribution to the CMB power spectrum is obtained following the same steps as above (see also Persi et al. 1995)

$$C_l^{(SZ)} = 32\pi^3 \left(\frac{\sigma_T}{m_e} \right)^2 \int_0^{\chi_0} \frac{a^2 d\chi}{r^2} P_p(k = l/r, \tau = \tau_0 - \chi),$$

(A.40)

where $P_p(k, \tau)$ is the power spectrum of electron pressure at time τ.

As a final example of Limber's equation I consider the transverse derivatives of the potential field, which are of interest in the discussion of gravitational lensing

(Appendix B). The radial integral is now of the form,

$$T_{ij} = \int_0^{\chi_0} W(\chi, \chi_0) \nabla_i \nabla_j \phi(\chi) d\chi \tag{A.41}$$

where $W(\chi, \chi_0)$ is again a broad smooth function. One can rewrite this using $\nabla_i = r^{-1} \partial_{\theta_i}$ into

$$T_{ij}(\vec{\theta}) = \partial_{\theta_i} \partial_{\theta_j} \int_0^{\chi_0} \frac{W(\chi, \chi_0)}{r^2} \phi(\chi) d\chi \equiv \partial_{\theta_i} \partial_{\theta_j} T(\vec{\theta}) \tag{A.42}$$

where $\vec{\theta}$ is the angular position in the sky. Fourier transform of $T(\vec{\theta})$ is given by

$$T(\vec{\theta}) = \int d^2\vec{l} \, e^{-i\vec{l} \cdot \vec{\theta}} T(\vec{l}), \tag{A.43}$$

where $\vec{l}$ is the two-dimensional wavevector. In Fourier space partial derivatives ∂_{θ_i} give angular wavevector l_i and this leads to

$$\langle T_{ij}(\vec{l}) T_{km}(\vec{l}') \rangle = l_i l_j l_k l_m \delta^2(\vec{l} - \vec{l}') \int_0^{\chi_0} \frac{W^2(\chi, \chi_0)}{r^6} P_\phi(l/r, \tau = \tau_0 - \chi) d\chi \tag{A.44}$$

and similarly for the first derivatives of ϕ,

$$\langle T_i(\vec{l}) T_j(\vec{l}') \rangle = l_i l_j \delta^2(\vec{l} - \vec{l}') \int_0^{\chi_0} \frac{W^2(\chi, \chi_0)}{r^4} P_\phi(l/r, \tau = \tau_0 - \chi) d\chi. \tag{A.45}$$

Bibliography

[1] Abbott, L. F., & Schaefer, R. K. 1986, ApJ, 308, 546

[2] Bardeen, J. 1980, Phys. Rev. D, 22, 1882

[3] Bertschinger, E. 1995, Les Houches Lecture Notes, to be published

[4] Bode, P., & Bertschinger, E. 1995, preprint astro-ph 9504040

[5] Bond, J. R., & Efstathiou, G. 1984, ApJ, 285, L45

[6] Kaiser, N. 1992, ApJ, 388, 272

[7] Kodama, H., & Sasaki, M. 1984, Prog. Theor. Phys. Suppl. 78, 1

[8] Kodama, H., & Sasaki, M. 1986, Int. J. Mod. Phys. A1, 265

[9] Limber, D. N. 1954, ApJ, 119, 655

[10] Ma, C. P., & Bertschinger, E. 1995, ApJ, to be published

[11] Peebles, P. J. E., The Large Scale Structure of the Universe (Princeton University, Princeton, NJ, 1980)

[12] Persi, F. M., Spergel, D. N., Cen, R., & Ostriker, J. P. 1995, ApJ, 442, 1

[13] Sunyaev, R. A., & Zel'dovich, Ya. B. 1980, ARA&A, 18, 357

[14] Vishniac, E. T. 1987, ApJ, 322, 597

[15] Wilson, M. L. 1983, ApJ, 273, 2

Appendix B

Gravitational Lensing in a Weakly Perturbed Robertson-Walker Universe

In this Appendix I present a general description of gravitational lensing in a weakly perturbed universe. The only assumption made is that of linearized gravity, $|\phi| \ll 1$. In particular, I do not assume that the density perturbations are small or that the lensing object is small compared to the distance to it. The equations are valid in a general Robertson-Walker universe and do not require the space to be flat (see also Pyne & Birkinshaw 1995).

B.1   Lens Equation and Time Delay

In an unperturbed universe a photon emitted from a source toward the observer will travel along a null geodesic in the radial direction with a radial position given by $\chi = \tau_0 - \tau$ (in this Appendix I use χ as the affine parameter instead of τ, because it leads to simplified expressions). Adding a perturbation changes the photon trajectory. The change in photon direction is governed by the space part of the geodesic equation

(A.4) applied to the metric (A.1), which gives (Bertschinger 1993),

$$\frac{d\vec{n}}{dl} = \vec{n} \times \left(\vec{n} \times \vec{\nabla}\right)\left(\psi + \phi - \vec{n} \cdot \overleftrightarrow{h} \cdot \vec{n}\right) + \vec{n} \times \left(\vec{\nabla} \times \vec{w} - \vec{n} \times \partial_r\vec{w}\right), \qquad \text{(B.1)}$$

where dl is the comoving differential photon pathlength. In the absence of vector $(\vec{w} = 0)$ and tensor perturbations $(\overleftrightarrow{h} = 0)$ and anisotropic stresses $(\phi = \psi)$ the above expression reduces to

$$\frac{d\vec{n}}{dl} = 2\vec{n} \times (\vec{n} \times \vec{\nabla}\phi) \equiv -2\vec{\nabla}_\perp\phi, \qquad \text{(B.2)}$$

where the symbol $\vec{\nabla}_\perp\phi$ denotes the transverse derivative of potential. Null geodesics obey $ds^2 = 0$, from which follows the relation $d\chi = (1 - 2\phi)dl$. Here ϕ can be interpreted as the Newtonian potential, since on scales smaller than the horizon it obeys the cosmological Poisson equation (equation A.11). It can be viewed as providing a force deflecting the photons and affecting their travel time while they propagate through the unperturbed space-time, described by a 3-sphere (closed universe), 3-hyperboloid (open universe) or Euclidean space (flat universe).

Equation (B.2) is a generalization of Einstein's deflection angle formula and includes the well-known factor of 2 difference compared to the Newtonian gravity. Even when metric perturbations are present, one can continue to parametrize the geodesic with the unperturbed comoving radial distance χ. The deflection angle at a given position χ can be calculated using a locally flat coordinate system, which allows a plane wave expansion for the potential ϕ, provided that the longest correlation length is small compared to the curvature length (this condition is probably well satisfied for the potential power spectrum in our universe). The effect of the deflection angle on the photon transverse position must however include the curvature effects. In practice this means that one has to solve triangles using the spherical, Euclidean or hyperboloid trigonometry. I shall adopt this quasi-Newtonian interpretation throughout the thesis. Because the only observable photon direction is that at the observer's position I will propagate photons relative to their final direction (i.e. backwards in time). I will also adopt a small deflection angle approximation, because one does not expect large deflection angles due to the lensing (see Chapter 4 for a more quantita-

tive justification of this approximation). This means that the transverse derivatives in equation (B.2) can be approximated with the transverse derivatives with respect to the observed direction of the photon or with respect to any other fiducial direction that has a small angular separation with the photon (for example the unperturbed direction to the source). In this spherical plane approximation the observed photon direction $\vec{n}$ can be described with a two-dimensional angle $\vec{\theta}$ with respect to the fiducial direction, $\vec{n} = (\theta_1, \theta_2, 1 - |\vec{\theta}|^2/2 \approx 1)$.

Suppose a photon is observed at an angle $\vec{\theta}$ relative to the source position. As it propagates through the universe the photon is additionally deflected according to equation (B.2) (see Figure B-1). This leads to the transverse photon excursion $\vec{x}_\perp(\chi)$ relative to the fiducial observer-source line. From Euclidean, spherical or hyperboloid trigonometry one finds that an individual deflection by $\delta\vec{\alpha}$ at χ' leads to an excursion at χ given by $\delta\vec{x}_\perp = \delta\vec{\alpha}\sin_K(\chi - \chi')$. The total excursion is given by an integral over individual deflections,

$$\vec{x}_\perp(\chi) = -2\int_0^\chi \vec{\nabla}_\perp \phi(\chi')\sin_K(\chi - \chi')d\chi' + \vec{\theta}\sin_K \chi. \tag{B.3}$$

The final photon direction $\vec{\theta}$ must be chosen so that the photon passes through the source position, $\vec{x}_\perp(\chi_S) = 0$, where χ_S is the radial distance to the source. This gives the lens equation

$$2\int_0^{\chi_S} \vec{\nabla}_\perp \phi(\chi)\sin_K(\chi_S - \chi)d\chi = \vec{\theta}\sin_K \chi_S. \tag{B.4}$$

This lens equation is valid for an arbitrary mass distribution between the source and the observer. For a given matter distribution it is an integral equation for $\vec{\theta}$ which can be solved, for example, using the ray-shooting method. For the special case of a single thin lens the photon is deflected by an angle $\vec{\alpha}$ at a lens position χ_L. This leads to the thin lens equation,

$$\sin_K \chi_S \vec{\theta} = -\sin_K(\chi_S - \chi_L)\vec{\alpha}, \tag{B.5}$$

which is equivalent to the lens equation expressed with angular diameter distances (e.g. Schneider, Ehlers & Falco 1992). The distances can be calculated for a given cosmological model using Friedman's equation (A.6) from the source redshift z_S and lens redshift z_L (assuming that the two redshifts can be measured). For example, for a flat universe without cosmological constant they are given by $\chi = 2H_0^{-1}[1-(1+z)^{-1/2}]$. I use the unperturbed comoving distance-redshift relation, because the deviations from it are $O(\phi)$ and can be neglected in the lowest order.

The time delay along the photon path relative to the unperturbed path can be decomposed into gravitational and geometrical parts $\Delta t = \Delta t_{\mathrm{grav}} + \Delta t_{\mathrm{geom}}$. The gravitational part is given by

$$\Delta t_{\mathrm{grav}} = -2 \int_0^{\chi_S} \phi(\chi')d\chi'. \tag{B.6}$$

The geometrical part is somewhat more complicated due to a curved geometry. One can slice the radial geodesic into n points at χ_i, separated by $\chi^{i+1} - \chi^i = \Delta\chi$. At each point a geodesic is constructed that is perpendicular to the radial geodesic and intersects the photon trajectory at a transverse position $\vec{x}^i_\perp$. The three geodesics together with the photon geodesic form a quadrilateral. Using spherical (Euclidean, hyperboloid) trigonometry one obtains the following expression for the geometrical time delay,

$$\Delta t_{\mathrm{geom}} = \int_0^{\chi_S} \frac{1}{2}\left[\left(\frac{\partial \vec{x}_\perp(\chi)}{\partial \chi}\right)^2 - K\vec{x}^2_\perp(\chi)\right] d\chi$$
$$\frac{\partial \vec{x}_\perp(\chi)}{\partial \chi} = -2 \int_0^{\chi} \cos_K(\chi - \chi')\vec{\nabla}_\perp \phi d\chi' + \vec{\theta}\cos_K \chi. \tag{B.7}$$

Again, for the particular case of a thin lens equations (B.6) and (B.7) reproduce the usual expression for the time delay.

B.2 Weak Lensing

Because of gravitational lensing the "true" surface brightness (i.e. the surface brightness one would see in the absence of any lensing) at position χ is mapped into the observed one, $I_{\mathrm{obs}}(\vec{\theta}) = I_{\mathrm{true}}(\vec{\theta} + \delta\vec{\theta})$, where $\delta\vec{\theta}$ is the angular deflection of a photon caused by intervening mass,

$$\delta\vec{\theta} = \frac{-2}{\sin_K \chi} \int_0^\chi \sin_K(\chi - \chi')\vec{\nabla}_\perp \phi(\chi')d\chi'. \tag{B.8}$$

While the deflection $\delta\vec{\theta}$ is not directly observable, its gradient is, through the stretching and magnification of distant galaxies. This is described by the two-dimensional shear tensor

$$\Phi_{ij} \equiv \frac{\partial \delta\theta_i}{\partial \theta_j} \approx \frac{-2}{\sin_K \chi} \int_0^\chi \sin_K(\chi - \chi')\sin_K \chi' \nabla_i \nabla_j \phi(\chi')d\chi'. \tag{B.9}$$

I Taylor expanded the potential in equation (B.8) across two neighbouring rays separated at the observer by $d\theta$ using the *unperturbed* separation $dx = \sin_K \chi' d\theta$. This approximation assumes that the shear Φ is small (Kaiser 1992), or, similarly, that the relative deflection between the neighboring rays is small compared to the unperturbed separation. This is the so-called weak lensing approximation and is implicitly assumed in most of the calculations in this thesis (the only exception being the strong lenses discussed in Chapter 4). While the validity of this approximation is not apriori guaranteed, it does seem to hold for most lines of sight in our universe. This is indicated by the rarity of strong lenses, where multiple images form and where shear is not small. More realistic estimates presented in Chapters 4 and 5 show that even in the extreme case where the source is placed at a high redshift the rms relative fluctuations between the photons do not exceed 20% for angular separations larger than an arcminute. Only on very small angular scales and for very distant sources might the weak lensing approximation break down, but this is a case of little observational relevance at the present time.

In equations (B.8) and (B.9) the potential derivative should be evaluated along

the perturbed path, but instead I will approximate it by evaluating it along the unperturbed path. For individual realizations of the potential field this is certainly not a good approximation, because a photon can stray away from its unperturbed path by more than a typical correlation length, as shown in Chapter 4. This is however of little concern here since one is not interested in individual realizations, but only in their statistical average over many random realizations. The statistical properties of the potential along the unperturbed paths are almost identical to those along the perturbed paths, as long as the pathlengths remain approximately equal.

For discussion of correlations in the shear or photon deflection between neighbouring rays it is convenient to introduce the correlation function $C(\theta)$, defined in equation (A.27). On small angular scales a sphere can be approximated with a plane and the correlation function can be rewritten in terms of the power spectrum C_l as

$$C(\theta) \approx \int \frac{d^2 \vec{l}}{(2\pi)^2} C_l \, e^{i\vec{l}\cdot\vec{\theta}}. \tag{B.10}$$

The sum over l in equation (A.27) was replaced with an integral $\int dl$, because for small angles (large l) l can be treated as a continuous variable. If there is no angular dependence in the power spectrum[1] C_l the above expression simplifies to

$$C(\theta) = \int \frac{l \, dl}{2\pi} C_l J_0(l\theta), \tag{B.11}$$

where $J_0(x)$ is the Bessel function of order 0.

Relative fluctuations between photons A and B separated by an angle θ at the observer's position (see Chapters 4 and 5) can be quantified using the correlation function C_{gl},

$$C_{gl}(\theta) = \langle \delta\vec{\theta}^A \cdot \delta\vec{\theta}^B \rangle_{\vec{\theta}^A \cdot \vec{\theta}^B = \cos\theta}. \tag{B.12}$$

---

[1]This is the case for all the calculations in this thesis, but need not be so if one is interested in the power spectrum of the shear field Φ_{ij} (Kaiser 1992).

From Limber's equation (A.45) and equations (B.8), (B.11) one obtains,

$$C_{gl}(\theta) = 16\pi^2 \int_0^\infty k^3 dk \int_0^{\chi_S} P_\phi(k, \tau = \tau_0 - \chi) W^2(\chi, \chi_S) J_0(k\theta \sin_K \chi) d\chi, \quad \text{(B.13)}$$

where χ_S is the source position and $W(\chi, \chi_S) = \sin_K(\chi_S - \chi)/\sin_K \chi_S$.

Similarly one can quantify the correlations in ellipticities of distant galaxies by introducing perpendicular and diagonal stretchings, $\chi_1 = \Phi_{11} - \Phi_{22}$ and $\chi_2 = 2\Phi_{12}$. Mean polarization p is defined as $\chi_1 + i\chi_2$. From equation (A.44) one obtains its autocorrelation function

$$C_{pp}(\theta) = 16\pi^2 \int_0^\infty k^5 dk \int_0^{\chi_g} P_\phi(k, \tau = \tau_0 - \chi) W^2(\chi, \chi_g)(\sin_K \chi)^2 J_0(k\theta \sin_K \chi) d\chi.$$
$$\text{(B.14)}$$

For simplicity I assumed a fixed distance to the background galaxies χ_g. A related quantity is the mean polarization $p(\theta)$, the average polarization within a circular aperture of radius θ, which also describes the correlations in the ellipticities of galaxy images as a function of angle θ. It is given by

$$p^2(\theta) = 16\pi^2 \int_0^\infty k^5 dk \int_0^{\chi_g} P_\phi(k, \tau = \tau_0 - \chi) W^2(\chi, \chi_g)(\sin_K \chi)^2 \left[\frac{2J_1(k\theta \sin_K \chi)}{k\theta \sin_K \chi} \right]^2 d\chi.$$
$$\text{(B.15)}$$

Equations (B.14) and (B.15) can also be used for calculating the correlations in magnification $m = \Phi_{11} + \Phi_{22}$.

B.3 Gravitational Lensing Effect on the CMB Correlation Function

Calculating the gravitational lensing effect on the CMB can be cumbersome in general, but it simplifies considerably if only small angular scales are considered and if the fluctuations in relative separation between the two photons can be considered gaussian. The first assumption is not very restrictive, since one does not expect the lensing effect to be important on large angular scales. The second assumption should

really limit the validity of the calculation to large scales only, where linear theory together with the assumption that initial fluctuations are gaussian guarantees its validity. In reality its validity extends beyond that to the quasi-linear scales, because the relative fluctuations are obtained by a projection of a 3-dimensional distribution over a broad radial window function and are in general much more gaussian than the 3-d distribution of the gravitational potential itself.

In the spherical plane approximation of equation (B.10) one can write the temperature anistropies in terms of Fourier transform,

$$\Delta_\gamma(\vec{\theta}) = \int d^2\vec{l}\, e^{-i\vec{l}\cdot\vec{\theta}} \Delta_\gamma(\vec{l}). \tag{B.16}$$

The correlation function including lensing is given by

$$\tilde{C}(\theta) = \langle \Delta_\gamma(\vec{\theta}^A + \delta\vec{\theta}^A)\Delta_\gamma(\vec{\theta}^B + \delta\vec{\theta}^B)\rangle_{\vec{\theta}^A\cdot\vec{\theta}^B=\cos\theta} =$$
$$= \int d^2\vec{l}\int d^2\vec{l}'\, e^{-i\vec{l}\cdot\vec{\theta}^A + i\vec{l}'\cdot\vec{\theta}^B}\, \langle e^{-i\vec{l}\cdot\delta\vec{\theta}^A + i\vec{l}'\cdot\delta\vec{\theta}^B}\Delta_\gamma(\vec{l})\Delta_\gamma^*(\vec{l}')\rangle, \tag{B.17}$$

where one has to average both over the intrinsic temperature anisotropies $\Delta_\gamma(\vec{l})$ and over lensing fluctuations $\delta\vec{\theta}$. The first averaging gives the angular power spectrum

$$\langle \Delta_\gamma(\vec{l})\Delta_\gamma^*(\vec{l}')\rangle = C_l\frac{\delta^2(\vec{l}-\vec{l}')}{(2\pi)^2}, \tag{B.18}$$

while the second gives the characteristic function of a gaussian field $\delta\vec{\theta}^A - \delta\vec{\theta}^B$,

$$\langle e^{-i\vec{l}\cdot(\delta\vec{\theta}^A - \delta\vec{\theta}^B)}\rangle = e^{-\sigma_{\Delta\theta}^2(\theta)l^2/2}, \tag{B.19}$$

where $\sigma_{\Delta\theta}(\theta)$ is the rms dispersion in the angular positions of the two photons,

$$\sigma_{\Delta\theta}^2(\theta) = \langle\left[\delta\vec{\theta}^A - \delta\vec{\theta}^B\right]^2\rangle_\theta = 2\left[C_{\rm gl}(0) - C_{\rm gl}(\theta)\right], \tag{B.20}$$

with $C_{gl}(\theta)$ given in equation (B.13). This leads to the modified correlation function

$$\tilde{C}(\theta) = (2\pi)^{-1} \int_0^\infty l\, dl\, e^{-\sigma^2_{\Delta\theta}(\theta)l^2/2} C_l J_0(l\theta). \qquad \text{(B.21)}$$

This equation is essentially the same as the Wilson & Silk (1981) expression for the correlation function observed with an instrument that has a gaussian beam profile, the only difference being that in the present case the dispersion $\sigma_{\Delta\theta}$ is dependent on angular separation. After another Fourier transform and using equation (6.615) from Gradshteyn & Ryzhik (1965) one obtains equation (5.1). Alternatively, one can also express the lensing effect directly in terms of the CMB power spectrum,

$$\tilde{C}_l = \int_0^\pi \theta d\theta \int_0^\infty l'\, dl'\, e^{-\sigma^2_{\Delta\theta}(\theta)l'^2/2} C_{l'} J_0(l\theta) J_0(l'\theta). \qquad \text{(B.22)}$$

Bibliography

[1] Bertschinger, E. 1993, in *Statistical Description of Transport in Plasma, Astro-, and Nuclear Physics*, ed. J. Misguich, G. Pelletier, & P. Schuck, (Commack, NY:Nova Science), p. 193 Frontières)

[2] Gradshteyn, I. S. & Ryzhik, I. M. 1965, Table of Integrals, Series and Products (New York:Academic)

[3] Kaiser, N. 1992, ApJ, 388, 272

[4] Pyne, T., & Birkinshaw, M. 1995, submitted to ApJ

[5] Schneider, P., Ehlers, J., & Falco, E. E. 1992, Gravitational Lenses (Springer-Verlag: New York)

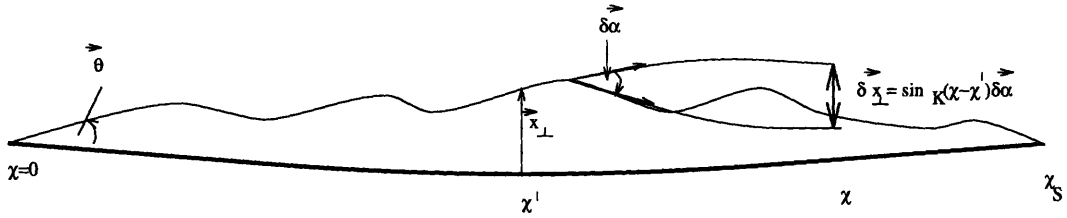[6] Wilson, M. L., & Silk, J. 1981, ApJ, 243, 14

Figure B-1: Photon propagation relative to the source-observer line. A photon is emitted at the source and observed at the observer's position in the direction $\vec{\theta}$ relative to the unperturbed source-observer direction (which is curved on an Euclidean plane because of background curvature). A deflection at χ' by $\delta\vec{\alpha} = -2\vec{\nabla}_{\perp}\phi\delta\chi$ leads to the transverse excursion at χ given by $\vec{\delta x}_{\perp}(\chi) = \sin_K(\chi - \chi')\delta\vec{\alpha}$. To satisfy the lens equation one must impose $\vec{x}_{\perp}(\chi_S) = 0$.